

Electronic Thesis and Dissertation Repository

12-13-2016 12:00 AM

The Efficacy of Bionate as an Articulating Surface for Joint Hemiarthroplasty

Sarah DeDecker, *The University of Western Ontario*

Supervisor: Dr. James Johnson, *The University of Western Ontario*

Joint Supervisor: Dr. Andrew Hrymak, *The University of Western Ontario*

A thesis submitted in partial fulfillment of the requirements for the Master of Engineering Science degree in Biomedical Engineering

© Sarah DeDecker 2016

Follow this and additional works at: <https://ir.lib.uwo.ca/etd>



Part of the [Biomaterials Commons](#)

Recommended Citation

DeDecker, Sarah, "The Efficacy of Bionate as an Articulating Surface for Joint Hemiarthroplasty" (2016). *Electronic Thesis and Dissertation Repository*. 4313.
<https://ir.lib.uwo.ca/etd/4313>

This Dissertation/Thesis is brought to you for free and open access by Scholarship@Western. It has been accepted for inclusion in Electronic Thesis and Dissertation Repository by an authorized administrator of Scholarship@Western. For more information, please contact wlsadmin@uwo.ca.

Abstract

Hemiarthroplasty procedures replace the diseased side of the joint with an implant to maximize bone preservation while maintaining more native anatomy than a total joint replacement. Even though hemiarthroplasty procedures have been clinically successful, they cause progressive cartilage damage over time due to the use of relatively stiff metallic implant materials. This work investigates the role of low moduli implant material on implant-cartilage contact mechanics and early *in vitro* cartilage wear. A finite element simulation was developed to assess the effect of low moduli implants in the range of 0.015-0.288 GPa on cartilage contact area and peak contact stress. Within the range of implant materials examined, higher contact area and lower peak contact stress was quantified as the Young's moduli decreased, particularly when the modulus was below 0.039 GPa. Bionate implants were then fabricated through microinjection moulding for three different Young's moduli of this biomaterial (0.020 GPa, 0.035 GPa and 0.222 GPa). An *in vitro* wear study was conducted using a pin-on-plate simulator to investigate the effect of these different Bionate formulations on cartilage wear. A significant decrease in cartilage wear was observed for the 0.020 GPa and 0.035 GPa Bionate implants ($p < 0.001$). In conclusion, these studies have demonstrated the desirable range of hemiarthroplasty implant moduli to reduce cartilage wear, and have shown that Bionate implants have the potential to provide improved long-term outcomes of joint hemiarthroplasty.

Keywords

Hemiarthroplasty, Bionate, polycarbonate urethane, cartilage wear, Young's modulus, biomaterials, biomechanics, contact area, contact stress

Co-Authorship Statement

Chapter One- sole authorship

Chapter Two

Study Design- Sarah DeDecker, James Johnson, Dan Langohr

Data Gathering- Sarah DeDecker, Dan Langohr

Writing- Sarah DeDecker

Revisions- Sarah DeDecker, James Johnson

Chapter Three

Study Design- Sarah DeDecker, James Johnson, Dan Langohr, Andrew Hrymak

Data Gathering- Sarah DeDecker, Dan Langohr

Writing- Sarah DeDecker

Revisions- Sarah DeDecker, James Johnson, Andrew Hrymak

Chapter Four

Study Design- Sarah DeDecker, Alana Khayat, Dan Langohr

Data Gathering- Sarah DeDecker

Data Analysis- Sarah DeDecker, Alana Khayat, Ryan Willing

Statistical Analysis- Sarah DeDecker, Dan Langohr

Writing- Sarah DeDecker

Revisions- Sarah DeDecker, James Johnson

Chapter Five- sole authorship

Acknowledgments

I would like to start off by thanking my supervisors, Dr. James Johnson and Dr. Andrew Hrymak. Dr. Johnson, you have provided me with so many opportunities to gain knowledge in orthopaedics and to grow as a researcher. You always gave me valuable advice and encouragement even when things got tough. I truly appreciate all the guidance and support you have given me during my research. Dr. Hrymak, you have given me valuable insight into the microinjection moulding process by sharing your extensive knowledge in this area. It has also been a pleasure working with Dr. Graham King and you are an inspiring surgeon and scientist.

I would also like to thank those who have been mentors to me throughout my research. Dr. Dan Langohr, thank you for always being there to answer my questions and sharing your vast knowledge with me. You dedicate so much of your time to help others and it does not go unnoticed. Alana Khayat, thank you for leading the way in wear testing. You inspired me to continue the research of material stiffness on contact mechanics in the hopes of improving hemiarthroplasty implants. Shengtai Zhou, you provided me with technical support and guidance on the microinjection moulding process. You were always generous with your time and extremely helpful.

I would like to thank my HULC and Chem Eng families. You are all very talented individuals and brought so much positivity to the lab and office every single day. You motivated me to work harder and strive for greatness.

Thank you DSM Biomedical for supplying me with the Bionate pellets. This research could not have been possible without this biomaterial. To Clayton and Ian at University Machine Services, thank you for making my mould vision become a reality. I know it was not an easy task developing the mould but in the end, it even exceeded my own expectations.

Finally, but certainly not last, I would like to thank my incredible and loving parents and sister. You encouraged me to keep moo-ving even through all the ups and downs that came with carrying out my research. I am so grateful that I got to share this journey with you and I am excited for the next chapter of my life.

Table of Contents

Abstract.....	i
Co-Authorship Statement.....	ii
Acknowledgments.....	iii
Table of Contents.....	iv
List of Tables	vii
List of Figures.....	viii
List of Abbreviations	x
Chapter 1.....	1
1.1 The Mechanical Function of Articular Cartilage.....	1
1.2 Hemiarthroplasty.....	3
1.3 Cartilage Wear	5
1.4 Bionate.....	6
1.4.1 Chemical Properties of Bionate	6
1.4.2 Mechanical Properties of Bionate.....	7
1.4.3 Bionate Implant Fabrication	8
1.4.4 Successful Bionate Applications.....	9
1.5 Biomechanical Studies of the Hemiarthroplasty Articulation	10
1.5.1 Finite Element Modeling of Hemiarthroplasty Implants Against Cartilage	10
1.5.2 Quantification of Cartilage Wear.....	11
1.6 Thesis Rationale.....	13
1.7 Objectives and Hypotheses.....	14
1.7.1 Objectives	14
1.7.2 Hypotheses.....	14
1.8 Thesis Overview	15

1.9	References.....	16
Chapter 2	25
	Implications of Low Stiffness Biomaterials on Contact Mechanics of Joint Hemiarthroplasty: A Finite Element Study.....	25
2.1	Introduction.....	25
2.2	Three-Dimensional Finite Element Modeling	26
2.2.1	The Model.....	26
2.3	Results.....	29
2.4	Discussion.....	34
2.5	Conclusion	35
2.6	References.....	36
Chapter 3	40
	Fabrication and Characterization of Bionate Implants.....	40
3.1	Introduction.....	40
3.2	Materials and Methods.....	41
3.2.1	Bionate Drying Conditions	41
3.2.2	Microinjection Moulding Conditions	41
3.3	Thermal Analysis of Bionate	46
3.3.1	Materials and Methods.....	46
3.3.2	Results.....	46
3.3.3	Discussion.....	49
3.4	Mechanical Properties of Bionate.....	51
3.4.1	Materials and Methods.....	51
3.4.2	Results.....	53
3.4.3	Discussion.....	56
3.5	Conclusion	56

3.6 References.....	57
Chapter 4.....	59
The Effect of Low Moduli Implant Biomaterials on Early <i>In Vitro</i> Cartilage Wear...	59
4.1 Introduction.....	59
4.2 Materials and Methods.....	60
4.2.1 Implant Models.....	60
4.2.2 Tissue Acquisition and Preparation	62
4.2.3 Wear Testing.....	63
4.2.4 Wear Quantification.....	63
4.3 Results.....	65
4.4 Discussion.....	70
4.5 Conclusion	72
4.6 References.....	73
Chapter 5.....	76
Conclusions and Recommendations	76
5.1 Findings Related to Objectives & Hypotheses	76
5.2 Recommendations for Future Work.....	77
5.3 Conclusions.....	78
Appendices.....	80
A. MeshLab Mesh Registration and MATLAB Volumetric Wear Calculation Protocols.....	80
B. Experimental Implant-Cartilage Contact Area Determined from an Experimental Casting Technique.....	83
Curriculum Vitae	85

List of Tables

Table 2-1: Summary of FEA results for varying implant moduli.....	30
Table 3-1: Battenfeld Microsystem 50 operating conditions.....	44
Table 3-2: TGA data of Bionate-Low, Bionate-Mid and Bionate-High.....	50
Table 3-3: DSC data of Bionate-Low, Bionate Mid and Bionate-High	51
Table 4-1: Surface roughness average for the four implant materials tested.....	62

List of Figures

Figure 1-1: Cross sectional diagram of the collagen fiber architecture in articular cartilage... 2

Figure 1-2: Hemiarthroplasty procedure involving a radial head replacement. (A) Lateral radiograph of a pre-operative radial head fracture in the right elbow; (B) Post-operative radiograph showing the radial head implant, which articulates against the humeral capitellum¹³ 4

Figure 2-1: Meshes and boundary conditions of the three-dimensional finite element model. All translation and rotation parallel to the cartilage surface were constrained. The pin was constrained in translation perpendicular to the cartilage surface at the guiding node. The subchondral bone guiding node was fully constrained. 27

Figure 2-2: Contact area and peak contact stress for the four implant materials..... 30

Figure 2-3: Compressive stress profiles on the cartilage surface for various implant models: a) Bionate-Low b) Bionate-Mid c) Bionate-High and d) ceramic 31

Figure 2-4: Contact areas at the implant-cartilage interface for various implant models: a) Bionate-Low b) Bionate-Mid c) Bionate-High and d) ceramic 32

Figure 2-5: Von Mises stress distribution at the implant-cartilage interface for various implant models: a) Bionate-Low b) Bionate-Mid c) Bionate-High and d) ceramic 33

Figure 3-1: a) Image of the cavity plate of the mould insert b) image of the other side of the mould insert c) schematic of final moulded Bionate pin 43

Figure 3-2: Schematic drawing of the microinjection moulding process: a) plasticization b) clamping c) moulding-holding and d) demoulding 45

Figure 3-3: TGA mass change curves for Bionate-Low, Bionate-Mid and Bionate-High..... 47

Figure 3-4: TGA first derivative of mass change curve for Bionate-Low, Bionate-Mid and Bionate-High..... 47

Figure 3-5: DSC analysis of Bionate-Low, Bionate-Mid and Bionate-High.....	48
Figure 3-6: Schematic of Bionate implant under compressive loading within the Instron	52
Figure 3-7: Mean (\pm one standard deviation) stress-strain curve for all three grades of Bionate	53
Figure 3-8: Mean (\pm one standard deviation) Young's moduli for Bionate-Low, Bionate-Mid and Bionate-High.....	55
Figure 4-1 Configuration of the pin-on-plate wear simulator: The Bionate pin was threaded on to the screw and coupling nut jig. A constant load of 30 N was applied to the cartilage surface via the implant model.	61
Figure 4-2: Mean (\pm one standard deviation) volumetric wear for: a) Bionate-Low b) Bionate-Mid c) Bionate-High and d) ceramic. Bionate-High and ceramic produced significantly more wear than Bionate-Low and Bionate-Mid ($p < 0.001$).	66
Figure 4-3: Mean (\pm one standard deviation) volumetric wear after 50,000 cycles for each implant material. Volumetric wear significantly increased between 10,000 and 50,000 cycles ($p < 0.05$).....	67
Figure 4-4: Mean (\pm one standard deviation) wear depth for: a) Bionate-Low b) Bionate-Mid c) Bionate-High and d) ceramic. Bionate-High and ceramic produced significantly deeper wear tracks in the cartilage plugs ($p < 0.001$).....	69
Figure A-1: MATLAB function to determine volumetric wear between unworn and worn surface meshes	82
Figure B-1: Mean (\pm one standard deviation) contact area measurements from casting for the four implant materials.....	84

List of Abbreviations

DSC	Differential scanning calorimetry
FEA	Finite element analysis
FSS	Friction shear stress
NMR	Nuclear magnetic resonance
PCU	Polycarbonate urethane
TGA	Thermogravimetric analysis
UHMWPE	Ultra high molecular weight polyethylene

Chapter 1

***Overview:** The treatise is on the subject of low modulus implant material selection for hemiarthroplasty, where the implant articulates against cartilage. This chapter provides an overview of the literature; with a focus on cartilage wear and using the biomaterial Bionate[®] as a proposed hemiarthroplasty implant material. It concludes with the objectives, hypotheses and thesis overview.*

1.1 The Mechanical Function of Articular Cartilage

Throughout joint motion, cartilage is subjected to friction, repeated loading, and traumatic injury. Hence, an understanding of the relevant mechanical properties is an important component in the study of cartilage function.

Cartilage is the viscoelastic and porous tissue that surrounds bone in synovial joints. Cartilage provides joints with essential functions which include load bearing, shock absorption, low friction, and wear resistance¹. The biphasic nature of cartilage helps to establish these properties (Figure 1-1). Cartilage consists of a solid and a fluid phase. The fluid phase makes up 60-80% of cartilage and is mostly composed of water. The solid phase is composed of strong collagen fibrils and proteoglycan (protein) macromolecules and is porous and permeable^{1,2}. Cartilage is comprised of four zones from the articulating surface to the underlying subchondral bone³:

- 1) The superficial zone includes tightly packed collagen fibers that are aligned parallel to the articular surface. This zone makes up 10-20% of articular cartilage volume and protects deeper layers from shear stresses.
- 2) The transitional zone includes proteoglycans and thicker collagen fibrils that are aligned obliquely. This zone represents 40-60% of articular cartilage volume and provides resistance to compressive forces.

3) The deep zone includes collagen fibrils that are aligned perpendicular to the articular surface. This zone represents 30% of articular cartilage volume and provides the greatest resistance to compressive forces. The deep zone contains the highest proteoglycan content and the lowest water concentration.

4) The calcified zone is needed to secure cartilage to bone by anchoring the collagen fibrils of the deep zone to the underlying subchondral bone.

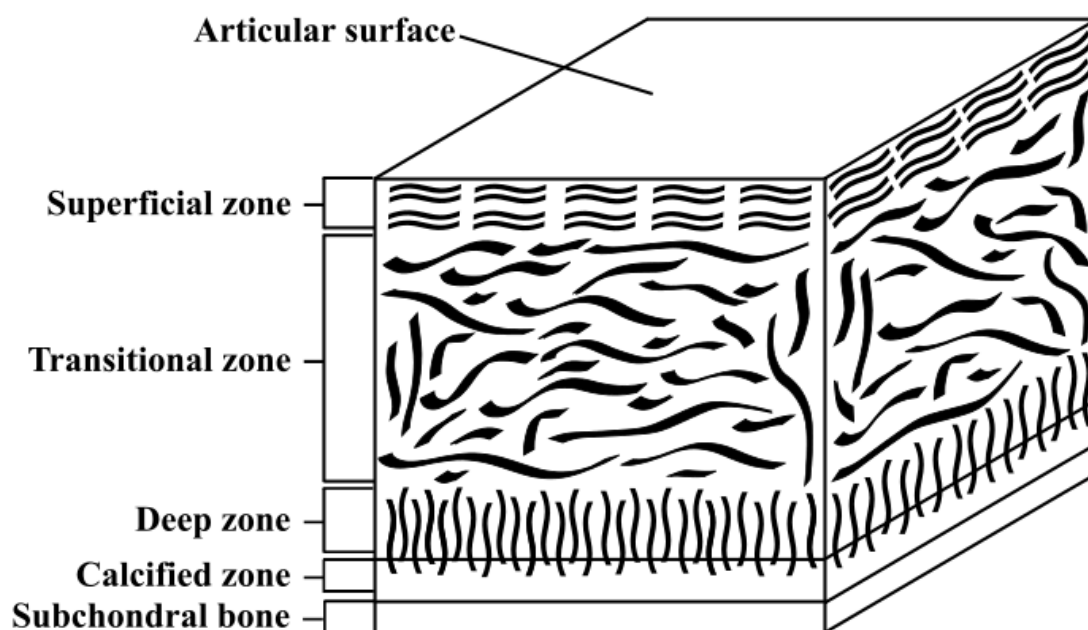


Figure 1-1: Cross sectional diagram of the collagen fiber architecture in articular cartilage

During compressive loading, the fluid phase carries most of the load and gradually flows out of the cartilage. The permeability of cartilage can be determined from a confined compression test and permeability is defined as the resistance to fluid flow through the cartilage matrix. Permeability is not constant through cartilage because of its multiphasic nature. The permeability is the highest near the joint surface and lowest in the deep zone where fibers are perpendicular to the articulating surface. Cartilage can withstand high compressive loads and the associated high shear and compressive stresses. Unconfined and confined compression testing is commonly used to evaluate the biomechanical

properties of articular cartilage⁴. The aggregate modulus of cartilage ranges from 0.50 to 0.90 MPa and the Young's modulus ranges from 0.45 to 0.80 MPa⁵. Another study reported a Young's modulus of 1.79 MPa⁶. Indentation tests have been used to determine the equilibrium and instantaneous Poisson's ratio of cartilage to be 0.46 and 0.50, respectively. The coefficient of friction for cartilage has been studied under static and dynamic loading. Higher values of 0.2-0.4 have been recorded for static loading over several hours, however under dynamic loading, the coefficient of friction ranges from 0.002-0.200⁷.

1.2 Hemiarthroplasty

Hemiarthroplasty procedures replace the diseased or damaged side of the joint with an implant to maximize bone preservation while maintaining more native anatomy than total joint replacement⁸. These procedures are typically performed due to pain and disability arising from focal cartilage erosion or from fractures resulting in an un-repairable joint. Hemiarthroplasty is preferred over total arthroplasty in fractures because it simplifies surgical procedure, preserves native bone and reduces costs^{9,10}. As an example, at the elbow, hemiarthroplasty is often employed as an option to treat complex radial head fractures because only one articulating surface in the joint is damaged (Figure 1-2)¹¹. The fractured radial head is removed and replaced with a metallic implant, which articulates against the native capitellum. The goals of radial head hemiarthroplasty are to restore elbow stability and preserve elbow motion¹². Clinical studies show promising outcomes for providing a functional range of motion and pain relief in hemiarthroplasty patients¹¹.

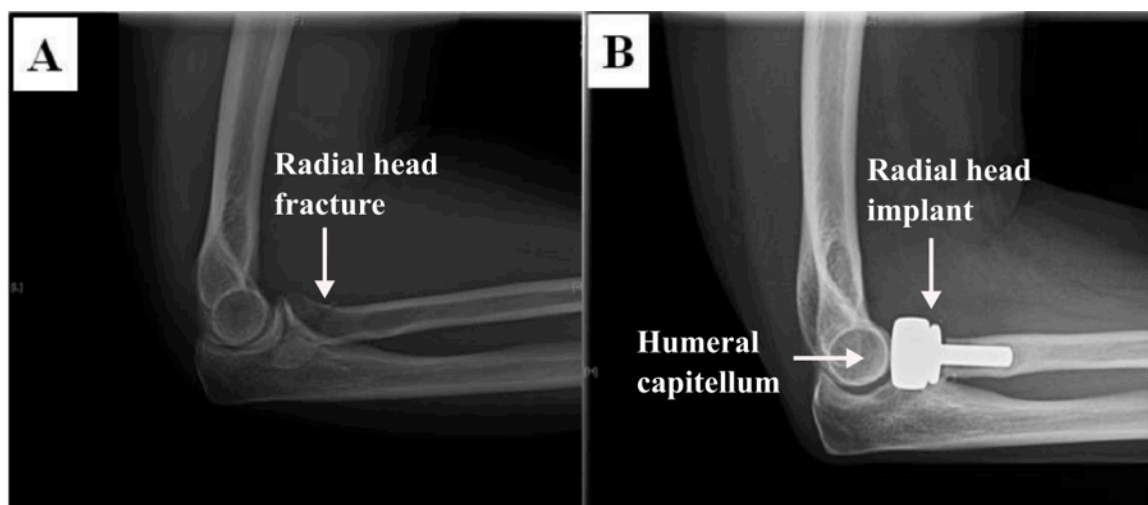


Figure 1-2: Hemiarthroplasty procedure involving a radial head replacement. (A) Lateral radiograph of a pre-operative radial head fracture in the right elbow; (B) Post-operative radiograph showing the radial head implant, which articulates against the humeral capitellum¹³.

Even though hemiarthroplasty procedures have been successful and have advantages as noted, they have been known to cause cartilage damage over time. It has been suggested by van Riet et al. that capitellar erosion occurs from metal radial head implants for the elbow. This is, in all likelihood due to the fact that the stiffness of the metallic implant is greater than that of cartilage. Hence, the contact area between the radial head and capitellum is decreased upon implantation relative to the native state¹⁴. Contact area in the radiocapitellar joint has been reported to decrease by two-thirds following metallic radial head arthroplasty which resulted in greater contact pressures within the joint¹⁵. Increased cartilage degradation is associated with elevated and unnatural contact pressures¹⁶. One mechanism that relates to cartilage degradation is the secretion of degenerative enzymes in articulating cartilage. These degenerative enzymes deteriorate the cartilage causing loss in elasticity and loss of surface integrity¹⁷.

In addition to metals, other materials that have been proposed and investigated to varied extents for hemiarthroplasty implants are polyvinyl alcohol hydrogels¹⁸ and polyurethane¹⁹. The Young's moduli of these materials are 0.7 MPa and 22 MPa, respectively. Polyvinyl alcohol hydrogels in as-gelled form have a high water content

which causes the hydrogels to lack the toughness and strength to serve as a cartilage substitute material²⁰⁻²². Thermal annealing has been used to strengthen hydrogels but by doing so decreases the lubricity of the hydrogel because the pores collapse within the hydrogel which causes damage to adjacent cartilage²³. Overall, hydrogels have less than desirable properties for implantation but polyurethane is a more desirable hemiarthroplasty material because it can reduce contact stress resulting in reduced levels of cartilage wear¹⁹.

1.3 Cartilage Wear

Wear is defined as the removal of material from the surface due to chemical or mechanical action between the contact surfaces⁷. Cartilage wear is a challenge to measure because the water content and biphasic properties vary in cartilage. Water content in the cartilage affects both geometric and gravimetric wear measurements. Studies have found changes in surface topography to be a better indication of surface damage caused by wear compared to gravimetric wear measurements⁷.

Weight bearing joints experience forces up to ten times body weight under normal loading conditions. These forces produce contact stresses in the range of 5-10 MPa²⁴. The compressive stress range of 15-20 MPa is the critical threshold stress that causes damage to the collagen fiber matrix in cartilage and causes chondrocyte death²⁴. Elevation of contact stress has been shown to increase friction at the implant-cartilage interface and causes an increase in cartilage wear. Friction shear stress (FSS) has been an important parameter in cartilage tribology studies and has demonstrated a very strong correlation between FSS and volume of cartilage wear^{25,26}. FSS is the product of contact stress and coefficient of friction.

With respect to hemiarthroplasty, contact stress was determined experimentally for three polyurethane tibial hemiarthroplasty bearings of varying stiffness²⁷. The two softer polymers produced contact stresses between 5 and 6 MPa. The higher stiffness polymer produced peak contact stresses around 16 MPa¹⁹. The polymers had much lower contact stress values compared to the conventional hemiarthroplasty material of stainless steel. Stainless steel produced the highest level of contact stress of 23 MPa¹⁹. Decreasing the

Young's moduli of the polyurethane tibial hemiarthroplasty bearings resulted in reduced levels of contact stress, therefore reducing levels of opposing cartilage wear¹⁹.

1.4 Bionate

The need to investigate Bionate[®], (DSM Biomedical, California, USA), a medical-grade polymer, in hemiarthroplasty applications is important because currently the stiffness of hemiarthroplasty implants is much higher than human cartilage. In fact, some early finite element work from our laboratory suggests that the modulus of an implant needs to be at least below 500 MPa before any discernible effects on cartilage stress and contact area occur²⁸. Hence, a low stiffness polymer such as Bionate has the potential to produce less cartilage wear on the native articulating surface while still maintaining implant longevity. Bionate demonstrates durability, biostability, flexibility, toughness, and biocompatibility making it a promising material for future hemiarthroplasty applications. In light of this, the work herein focuses on Bionate.

1.4.1 Chemical Properties of Bionate

Bionate is a polycarbonate urethane (PCU). Polycarbonate urethanes are synthesized at the molecular level using a hydroxyl terminated polycarbonate, an aromatic diisocyanate and a chain extender²⁹. Bionate is specifically made from poly(hexamethylene carbonate), methylene di(p-phenyl isocyanate) and butanediol. The polycarbonate is the soft segment of the polymer and provides stability. The polyurethane is the hard segment of the polymer and provides strength³⁰. The chain extender cross-links the two segments together to create Bionate. For example, Bionate 80A has a hard-to-soft segment ratio of 35/65 (wt/wt)³⁰.

Bionate has the ability to imitate one of the roles of natural cartilage by offering a high degree of compliance to promote fluid-film lubrication³¹. Previously conducted wear studies have shown Bionate to have superior wear and friction characteristics compared to traditional metal against ultra high molecular weight polyethylene (UHMWPE) devices when considered for total joint replacement systems³².

Bionate has outstanding ageing and hydrolysis resistance. Bionate gets its high oxidative stability from its chemical structure, the proximity of the hydrocarbon groups to the carbonate linkages²⁹. Oxidative stability helps prevent irreversible changes from occurring in the polymer's properties, known as ageing. *In-vitro* studies have assessed Bionate's resistance to degradation mechanism such as environmental stress cracking and metal ion oxidation^{33,34}.

1.4.2 Mechanical Properties of Bionate

The hardness of Bionate is measured on the Shore A or Shore D scale, where A is softer than the D scale. The softer grades of Bionate are 80A and 90A. The harder grades of Bionate are 55D, 65D, and 75D. Polycarbonate urethane elastomers are considered "cushion bearing" in orthopaedic implant applications¹⁹. PCU has high abrasion and tear resistance and flexural fatigue life³⁵.

Coefficient of friction testing (using ASTM D1894) has been conducted on Bionate 80A, 55D, and 75D with the kinetic coefficient of friction being 1.52, 0.81, and 0.64, respectively³⁶. Bionate 80A has a coefficient of friction greater than 1 which means the frictional force is greater than the normal force.

Ghaill et al.³⁷ conducted volumetric compression testing of Bionate 80A and Bionate 75D to determine the bulk modulus, Young's modulus, and Poisson's ratio. For Bionate 80A, over 10 loading cycles, the bulk modulus increased from 497.1 MPa to 524.2 MPa and the Young's modulus increased from 22.19 MPa to 23.93 MPa. The Poisson's ratio was 0.49. For Bionate 75D, over 10 loading cycles, the bulk modulus increased from 292.9 MPa to 472.3 MPa and the Young's modulus increased from 131.1 MPa to 327.6 MPa. The Poisson's ratio ranged decreased from 0.43 to 0.38³⁷. Bionate 80A has also been reported to have a Young's modulus of 19.2 MPa³⁸ and ranging in Young's modulus between 28 and 30 MPa³⁰.

The Young's modulus of Bionate 55D has been documented. Simmons et al. studied unstrained non-implanted controls that were compared to samples that were implanted into an ovine model for 12 months³⁹. Tensile mechanical testing was conducted to

determine the Young's modulus of implanted and non-implanted samples. The non-implanted samples were unstrained while the implanted samples were strained at 150% for the 12-month testing period. The Young's modulus for the implanted samples was 134.8 ± 6.3 MPa. The Young's modulus for the non-implanted controls was 39.2 ± 3.2 MPa³⁹. This data indicated that the implanted samples were less extensible and flexible when compared to the non-implanted samples, which has been reported from other studies. This change in elastic modulus is attributed to a combination of chain orientation, stress relaxation, and strain-induced crystallization within the polymer⁴⁰.

1.4.3 Bionate Implant Fabrication

Injection moulding has been used to mould Bionate for several total arthroplasty applications including shoulder glenoid components³¹, hip acetabular cups⁴¹, knee tibial bearing inserts⁴², and spinal implants⁴³.

Bionate is packaged in polymer pellet form. Moisture level within the pellets is a key factor before injection moulding because it can impact the quality and ability to be processed into moulded parts. To reduce pellet moisture level, the pellets are dried before being moulded into the desired implant shape.

The injection moulding process can be categorized into four stages: plasticization, clamping, moulding-holding, and demoulding⁴⁴. Raw solid polymer pellets are placed into the hopper of the injection-moulding machine. The pellets travel through the hopper and into the barrel where plasticization occurs. Heat is supplied to the pellets by heater bands around the barrel and from the mixing action that occurs from the screw rotating within the barrel. The pellets are turned into a continuous liquid melt based on mechanical and thermal energy⁴⁵. The screw component produces homogenous and efficient plasticization. The melted polymer then travels into a metering barrel to a preset volume to help create consistent processing through heat transfer and melt flow. The mould is then pressed together and the injection plunger forces the metered melt into the injection unit⁴⁶. Cooling time occurs before the mould can open and release the moulded part.

Geary et al. used injection moulding to create rectangular Bionate 80A and Bionate 75D tiles²⁹. Gel permeation chromatography was used to determine the optimal drying temperature of the raw Bionate pellets and the optimal moulding temperature. Optimal drying was achieved after 12 hours in a fan-assisted oven at 80°C. Moulding temperatures were performed at 200, 220, and 240°C but for optimal moulding, the temperature should not exceed 220°C²⁹.

1.4.4 Successful Bionate Applications

One of the major causes of failure in joint replacements is implant wear. Wear of implant materials such as metals and UHMWPE cause wear particles/wear debris which can lead to bone resorption and loosening of the implant. UHMWPE is used in total joint arthroplasty in orthopaedic and spine implants because of its resistance to wear. Polyurethane has been used in high resiliency applications such as intervertebral disc replacement implants and implantable artificial heart valves because of its mechanical and biocompatibility properties³⁵. Polycarbonate urethane has been recommended as an alternative bearing material for the acetabular cup³⁵. Wear particles of polycarbonate urethane are less inflammatory compared to UHMWPE and therefore potentially less disruptive to bone-implant fixation and other side effects^{47,48}. Some authors speculate that this difference is caused by PCU being hydrophilic and UHMWPE is hydrophobic. In a study conducted by Geary et al., lower wear rates were observed for PCU compared to UHMWPE³¹.

Studies have been conducted to evaluate polycarbonate urethane acetabular cup wear performance. The PCU cups were tested in an ovine arthroplasty model and showed the effectiveness of PCU biostability over periods as long as 48 months. The cups had no apparent changes in material or evidence of degradation⁴⁹⁻⁵¹. Another study showed polyurethane to be superior over UHMWPE in knee prosthesis with cement fixation during wear, friction and creep testing⁵². A study conducted by Smith et al. used gravimetric analysis to measure the wear of five polyurethane acetabular cups and calculated the average wear rate as $12.0 \pm 3.6 \text{ mm}^3/\text{million cycles}$. Creep rather than wear caused the large spread in the data (calculated standard deviation values)⁵². Carbone et al. conducted an *in vivo* study to investigate the wear of PCU bearing in an ovine total hip

arthroplasty model for up to four years⁵⁰. The study found no surface damage or deterioration of the PCU compliant layer^{49,50}.

Dynamic compression fatigue tests were performed on Bionate compliant layer acetabular cups and tibial bearings, which were positioned in fixtures attached to a servohydraulic fatigue-testing machine. Bionate 75D was used for the backing of the two components and Bionate 80A was used as the compliant layer. The tests were performed under 14.4×10^6 cycles and caused no visible damage or debonding between the Bionate 80A and Bionate 75D interface. The study concluded that using soft and hard PCU materials for acetabular components and tibial bearings are reliable and strong enough to withstand robust mechanical testing⁵³.

There is less understanding on the effectiveness of PCU, specifically Bionate, as a hemiarthroplasty material because most of the studies have been on total joint replacement. PCU has produced favourable results as an alternative implant material when articulating against another material such as metal, but it is still unclear how PCU articulates against native cartilage.

1.5 Biomechanical Studies of the Hemiarthroplasty Articulation

1.5.1 Finite Element Modeling of Hemiarthroplasty Implants Against Cartilage

In vivo contact stresses and strains are difficult to measure experimentally and often inaccurate in synovial joints⁵⁴. Since the 1970s computational simulations have helped to effectively determine contact stresses, contact areas, and strains in orthopaedic biomechanical applications⁵⁵. Finite element analysis (FEA) involves discretizing complex, continuous geometries into smaller elements or meshes. The elements are solved and assembled to determine local strains and stresses of the elements. Finite element analysis has been used to characterize articular contact mechanics in the shoulder⁵⁶, the elbow⁵⁷⁻⁶⁰, the hip^{61,62}, the knee^{63,64}, and amongst others.

Finite element analysis has been used to characterize mechanical responses of structures. Articular cartilage has been successfully modeled using a finite element model. Cartilage was first modeled as a linear elastic model but has evolved to biphasic analytical models. Early analytical models of deformation of cartilage were single phase, linear elastic solids where time dependent behaviour was not accounted for. Unfortunately this is not an ideal representation for all physiological loading⁶⁵. Instantaneous response of hyperelastic material has been shown to have the equivalent response of biphasic material under fast loading conditions⁶¹ and therefore articular cartilage is better represented when modeled as an incompressible, neo-Hookean hyperelastic material^{61,62,66,67}.

Cilingir et al., studied contact pressure in a hemiarthroplasty hip joint using three-dimensional anatomic, two-dimensional axisymmetric and three-dimensional axisymmetric finite element models⁶⁸. It was concluded that axisymmetric models have good agreement with anatomic models and therefore can be used for contact mechanics studies and require less computational time⁶⁸.

Polycarbonate urethane has been modeled as an incompressible, Mooney-Rivlin hyperelastic material^{69,70}. The finite element model was validated by comparing the tibial plateau contact pressures measured in *in vitro* cadaveric knee experiments to the calculated contact pressures determined from the finite element analysis. Therefore, finite element analysis can be used to simulate hemiarthroplasty implant-cartilage contact mechanics and can enhance *in vitro* wear results by determining stress distributions, contact area, contact pressure, and peak contact stress.

1.5.2 Quantification of Cartilage Wear

McGann et al. studied methods to assess *in vitro* wear of articular cartilage by conducting wear testing of cartilage against stainless steel discs⁷¹. The three methods they used were: assessing collagen wear in the cartilage specimen by using a modified wear factor, quantifying surface damage by making the damage visible by India ink, and measuring changes in surface roughness⁷¹. During wear testing, the bovine specimens released cartilage wear debris into the lubricating bath. Liquid chromatography was used to measure changes in protein content of the lubricating bath. The wear factor (mg/N-m) of

each specimen was determined by dividing the mass of cartilage removed (amount of hydroxyproline in the lubrication bath) by the load applied during wear testing and the total length the specimen traveled within the pin-on-disc wear machine. Surface roughness of the cartilage surface was measured before and after wear testing, and was found to be an ineffective measure of cartilage degradation. The results showed a general trend of increasing surface roughness after wear testing but the surface roughness did not correlate with the modified wear factor. Changes in surface morphology of the cartilage may not be captured by the surface roughness measurement⁷¹. However, India ink was found to be an effective, inexpensive and quick technique for evaluating cartilage degradation.

Lizhang et al. studied the effect of contact stress and area on cartilage wear in a hemiarthroplasty application. The study showed an increase in contact stress when the contact area was decreased⁷². In another investigation, Lizhang et al. studied the effect of contact stress and area, sliding speed and distance, and loading time on cartilage deformation, friction and wear. Bovine cartilage pins were reciprocated against cobalt chromium alloy plates to mimic hemiarthroplasty articulation. Cartilage wear increased with sliding speed and distance, and contact stress⁷.

Tribological simulation was developed to determine wear and friction properties of bovine knee articular cartilage against cartilage and cartilage against stainless steel by applying physiological loads and motions to the knee joints. Joint contact stress was measured using pressure sensitive Fuji film. The film was placed between the hemiarthroplasty material (stainless steel) and cartilage and the pendulum friction simulator applied the required load⁷³. The study concluded that under high loading conditions, coefficient of friction is not a good indicator of cartilage wear, but did demonstrate that contact stress is an important factor influencing cartilage wear. Contact stress at the interface was much higher for cartilage-stainless steel interaction and resulted in more cartilage wear when compared to cartilage-cartilage interaction.

Recent work in our laboratory by Khayat, involved quantifying cartilage wear by comparing three-dimensional scans of articular cartilage taken before and after pin-on-

disc wear testing¹³. India ink was added to the cartilage surface to help visualize the wear track. The pre- and post- wear scans were aligned in MeshLab and a custom inter-surface distance MATLAB algorithm was used to determine volumetric wear. The distance between the vertices of the triangular meshes determined volumetric wear. The unworn regions of the mesh had a distance of zero because the vertices of the aligned meshes had the same coordinates. The distance between corresponding points on the registered surfaces determined the worn regions. This method was deemed an effective non-contact imaging protocol to quantify cartilage surface and wear damage.

1.6 Thesis Rationale

Hemiarthroplasty is a minimally invasive procedure that maximizes the preservation of native anatomy and restores joint kinematics, function and stability. While these procedures are initially highly successful, cartilage wear leads to clinical failures with longer follow-up. To optimize load transfer and improve clinical outcomes, hemiarthroplasty implants must improve articular contact mechanics by decreasing contact stress and therefore minimizing articular cartilage wear at the implant-cartilage interface.

The literature suggests that a more compliant material should be used in hemiarthroplasty implants because they may reduce cartilage degeneration^{19,74,75}. More compliant implant materials have shown to produce less wear but the relationship between implant stiffness and articular cartilage damage remains unclear. It is not well known whether there is a gradual increase in articular cartilage wear as implant stiffness increases, or if there is a threshold level where contact mechanics shift to cause harm to the cartilage, particularly for the lower modulus materials such as Bionate.

In view of the foregoing, the success of a more compliant hemiarthroplasty implant using Bionate was studied. Contact area at the implant-cartilage interface will be compared between *in vitro* wear tests and computational finite element analysis. These studies were conducted to explain the relationship between low stiffness biomaterials and cartilage wear. *In vitro* studies utilized a pin-on-plate wear simulator that reciprocated low stiffness hemiarthroplasty implant models against fresh frozen bovine articular cartilage

explants. Volumetric wear was determined from topographical changes in the cartilage surfaces. Finite element simulations will be used to determine contact stresses and contact area at the implant-cartilage interface.

1.7 Objectives and Hypotheses

1.7.1 Objectives

1. To develop and employ a finite element model to assess the effect of low modulus implants in the range of 0.015-0.288 GPa on cartilage contact area and peak contact stress.
2. To develop an efficient and effective way to fabricate Bionate hemispherical-tipped implants and to characterize the chemical and mechanical properties of Bionate implants.
3. To quantify the effect of varying Bionate implant stiffness on early *in vitro* cartilage wear.

1.7.2 Hypotheses

1. Finite element model will show an increase in contact area and a decrease in peak contact stress at the implant-cartilage interface with a decrease in implant moduli (Chapter 2).
2. It is hypothesized that decreasing the implant stiffness will reduce wear on the adjacent cartilage because of improved contact mechanics (Chapter 4).

1.8 Thesis Overview

The following chapters represent a comprehensive collection of computational and experimental studies to investigate the effect of low modulus biomaterial (*viz.* Bionate). A finite element study was initially conducted to determine the effect of low stiffness material on contact mechanics (contact area and peak contact stress). Chapter 3 focuses the fabrication of Bionate 80A (referred to as Bionate-Low in the following chapters), 55D (Bionate-Mid), and 75D (Bionate-High) implants and chemical and mechanical characterization of the various implants. Chapter 4 presents the effect of Bionate implants on early *in vitro* cartilage wear using a pin on cartilage model. Chapter 5 summarizes the conclusions and direction of future research.

1.9 References

1. Xin L, Lu VCM. Biomechanics of Articular Cartilage and Determination of Material Properties. *Med Sci Sports Exerc.* 2008;40(2):193–9. DOI: 10.1249/mss.0b013e31815cb1fc.
2. Mansour JM, Mow VC. The permeability of articular cartilage under compressive strain and at high pressures. *J Bone Jt Surg.* 1976;58(4):509–16.
3. Sophia Fox AJ, Bedi A, Rodeo SA. The Basic Science of Articular Cartilage. *Sports Health.* 2009;1(6):461–8. DOI: 10.1177/1941738109350438.
4. Boschetti F, Pennati G, Gervaso F, Peretti GM, Dubini G. Biomechanical properties of human articular cartilage under compressive loads. *Biorheology.* 2004;41(3–4):159–66.
5. Mansour JM. Biomechanics of Cartilage. *Kinesiology: the mechanics and pathomechanics of human movement*, vol. 2. 2004. p. 66–79.
6. Jin H, Lewis JL. Determination of Poisson's Ratio of Articular Cartilage by Indentation Using Different-Sized Indenters. *J Biomech Eng.* 2004;126(2):138–45. DOI: 10.1115/1.1688772.
7. J Lizhang JF. The effect of contact stress on cartilage friction, deformation and wear. *Proc Inst Mech Eng [H].* 2011;225(5):461–75. DOI: 10.1177/2041303310392626.
8. Klaus J, Burkhart SN. Distal Humerus Hemiarthroplasty of the Elbow for Comminuted Distal Humeral Fractures in the Elderly Patient. *J Trauma.* 2011;71(3):635–42. DOI: 10.1097/TA.0b013e318216936e.
9. Liu J, Li S, Cai Z, Lou L, Wu X, Zhu Y, et al. Outcomes, and factors affecting outcomes, following shoulder hemiarthroplasty for proximal humeral fracture repair. *J Orthop Sci.* 2011;16(5):565–72. DOI: 10.1007/s00776-011-0113-8.

10. van der Meulen MCH, Beaupré GS, Smith RL, Giddings VL, Allen WA, Athanasiou KA, et al. Factors influencing changes in articular cartilage following hemiarthroplasty in sheep. *J Orthop Res*. 2002;20(4):669–75. DOI: 10.1016/S0736-0266(01)00182-6.
11. Shore BJ, Mozzon JB, MacDermid JC, Faber KJ, King GJW. Chronic Posttraumatic Elbow Disorders Treated with Metallic Radial Head Arthroplasty. *J Bone Jt Surg*. 2008;90(2):271–80. DOI: 10.2106/JBJS.F.01535.
12. Calfee R, Madom I, Weiss A-PC. Radial Head Arthroplasty. *J Hand Surg*. 2006;31(2):314–21. DOI: 10.1016/j.jhsa.2005.12.005.
13. Khayat A. Effect of Hemiarthroplasty Implant Contact Geometry and Material on Early Cartilage Wear. *Electron Thesis Diss Repos*. 2015.
14. van Riet RP, Glabbeek FV, Verborgt O, Gielen J. Capitellar Erosion Caused by a Metal Radial Head Prosthesis. *J Bone Jt Surg Am*. 2004;86(5):1061–4.
15. Liew VS, Cooper IC, Ferreira LM, Johnson JA, King GJW. The effect of metallic radial head arthroplasty on radiocapitellar joint contact area. *Clin Biomech*. 2003;18(2):115–8. DOI: 10.1016/S0268-0033(02)00172-9.
16. McGibbon CA, Krebs DE, Trahan CA, Trippel SB, Mann RW. Cartilage degeneration in relation to repetitive pressure: Case study of a unilateral hip hemiarthroplasty patient. *J Arthroplasty*. 1999;14(1):52–8. DOI: 10.1016/S0883-5403(99)90202-4.
17. Moon KH, Kang JS, Lee TJ, Lee SH, Choi SW, Won MH. Degeneration of Acetabular Articular Cartilage to Bipolar Hemiarthroplasty. *Yonsei Med J*. 2008;49(5):719–24. DOI: 10.3349/ymj.2008.49.5.719.
18. Nakashima K, Sawae Y, Tsukamoto N, Miura H, Iwamoto Y, Murakami T. Wear Behaviour of an Artificial Cartilage Material for Hemiarthroplasty. In: Lim CT, and Goh JCH, editors. *6th World Congress of Biomechanics (WCB 2010). August 1-6, 2010 Singapore*. Springer Berlin Heidelberg; 2010. p. 1169–72.

19. Luo Y, McCann L, Ingham E, Jin Z-M, Ge S, Fisher J. Polyurethane as a potential knee hemiarthroplasty biomaterial: An in-vitro simulation of its tribological performance. *Proc Inst Mech Eng [H]*. 2010;224(3):415–25. DOI: 10.1243/09544119JEIM657.
20. Azuma C, Yasuda K, Tanabe Y, Taniguro H, Kanaya F, Nakayama A, et al. Biodegradation of high-toughness double network hydrogels as potential materials for artificial cartilage. *J Biomed Mater Res A*. 2007;81A(2):373–80. DOI: 10.1002/jbm.a.31043.
21. Peppas NA, Merrill EW. Development of semicrystalline poly(vinyl alcohol) hydrogels for biomedical applications. *J Biomed Mater Res*. 1977;11(3):423–34. DOI: 10.1002/jbm.820110309.
22. Stammen JA, Williams S, Ku DN, Guldborg RE. Mechanical properties of a novel PVA hydrogel in shear and unconfined compression. *Biomaterials*. 2001;22(8):799–806. DOI: 10.1016/S0142-9612(00)00242-8.
23. Bodugoz-Senturk H, Choi J, Oral E, Kung JH, Macias CE, Braithwaite G, et al. The effect of polyethylene glycol on the stability of pores in polyvinyl alcohol hydrogels during annealing. *Biomaterials*. 2008;29(2):141–9. DOI: 10.1016/j.biomaterials.2007.09.015.
24. Torzilli PA, Grigiene R, Borrelli J J, Helfet DL. Effect of Impact Load on Articular Cartilage: Cell Metabolism and Viability, and Matrix Water Content. *J Biomech Eng*. 1999;121(5):433–41. DOI: 10.1115/1.2835070.
25. McCann L, Ingham E, Jin Z, Fisher J. Influence of the meniscus on friction and degradation of cartilage in the natural knee joint. *Osteoarthritis Cartilage*. 2009;17(8):995–1000. DOI: 10.1016/j.joca.2009.02.012.
26. McCann L, Ingham E, Jin Z, Fisher J. An investigation of the effect of conformity of knee hemiarthroplasty designs on contact stress, friction and degeneration of articular cartilage: A tribological study. *J Biomech*. 2009;42(9):1326–31. DOI: 10.1016/j.jbiomech.2009.03.028.

27. Luo Y, McCann L, Ingham E, Jin Z-M, Ge S, Fisher J. Polyurethane as a potential knee hemiarthroplasty biomaterial: An in-vitro simulation of its tribological performance. *Proc Inst Mech Eng [H]*. 2010;224(3):415–25. DOI: 10.1243/09544119JEIM657.
28. Johnson A, Langohr DG, King GJW, Johnson JA. The Effect of Radial Head Hemiarthroplasty Stiffness on Joint Contact Mechanics. 2015.
29. Geary C, Birkinshaw C, Jones E. Characterisation of Bionate polycarbonate polyurethanes for orthopaedic applications. *J Mater Sci Mater Med*. 2008;19(11):3355–63. DOI: 10.1007/s10856-008-3472-8.
30. Wiggins MJ, MacEwan M, Anderson JM, Hiltner A. Effect of soft-segment chemistry on polyurethane biostability during in vitro fatigue loading. *J Biomed Mater Res A*. 2004;68A(4):668–83. DOI: 10.1002/jbm.a.20081.
31. Geary C, Jones E, Fitzpatrick D, Kelly CP, Birkinshaw C. In-vitro evaluation of a polyurethane compliant-layer glenoid for use in shoulder arthroplasty. *Proc Inst Mech Eng [H]*. 2010;224(4):551–63. DOI: 10.1243/09544119JEIM626.
32. Scholes SC, Unsworth A, Blamey JM, Burges IC, Jones E, Smith N. Design aspects of compliant, soft layer bearings for an experimental hip prosthesis. *Proc Inst Mech Eng [H]*. 2005;219(2):79–87. DOI: 10.1243/095441105X9318.
33. Tanzi MC, Mantovani D, Petrini P, Guidoin R, Laroche G. Chemical stability of polyether urethanes versus polycarbonate urethanes. *J Biomed Mater Res*. 1997;36(4):550–9. DOI: 10.1002/(SICI)1097-4636(19970915)36:4<550::AID-JBM14>3.0.CO;2-E.
34. Tanzi MC, Farè S, Petrini P. In vitro stability of polyether and polycarbonate urethanes. *J Biomater Appl*. 2000;14(4):325–48.
35. St John K, Gupta M. Evaluation of the wear performance of a polycarbonate-urethane acetabular component in a hip joint simulator and comparison with UHMWPE and cross-linked UHMWPE. *J Biomater Appl*. 2012;27(1):55–65. DOI: 10.1177/0885328210394471.

36. DSM. Bionate Thermoplastic Polycarbonate Polyurethane (PCU). Available at [http://www.dsm.com/content/dam/dsm/medical/en_US/documents/bionate\(r\)-pcu-product-sheet.pdf](http://www.dsm.com/content/dam/dsm/medical/en_US/documents/bionate(r)-pcu-product-sheet.pdf).
37. Ghail NNA, Little EG. Determination of the mechanical properties of Bionate 80A and Bionate 75D for the stress analysis of cushion form bearings. *Proc Inst Mech Eng [H]*. 2008;222(5):683–94. DOI: 10.1243/09544119JEIM372.
38. Jones E, Scholes SC, Unsworth A, Burgess IC. Compliant-layer tibial bearing inserts: Friction testing of different materials and designs for a new generation of prostheses that mimic the natural joint. *Proc Inst Mech Eng [H]*. 2008;222(8):1197–208. DOI: 10.1243/09544119JEIM442.
39. Simmons A, Hyvarinen J, Odell RA, Martin DJ, Gunatillake PA, Noble KR, et al. Long-term in vivo biostability of poly(dimethylsiloxane)/poly(hexamethylene oxide) mixed macrodiol-based polyurethane elastomers. *Biomaterials*. 2004;25(20):4887–900. DOI: 10.1016/j.biomaterials.2004.01.004.
40. Hergenrother RW, Wabers HD, Cooper SL. Effect of hard segment chemistry and strain on the stability of polyurethanes: in vivo biostability. *Biomaterials*. 1993;14(6):449–58. DOI: 10.1016/0142-9612(93)90148-U.
41. Scholes SC, Burgess IC, Marsden HR, Unsworth A, Jones E, Smith N. Compliant Layer Acetabular Cups: Friction Testing of a Range of Materials and Designs for a New Generation of Prosthesis that Mimics the Natural Joint. *Proc Inst Mech Eng [H]*. 2006;220(5):583–96. DOI: 10.1243/09544119H06404.
42. Flannery M, Flanagan S, Jones E, Birkinshaw C. Compliant layer knee bearings: Part I: Friction and lubrication. *Wear*. 2010;269(5–6):325–30. DOI: 10.1016/j.wear.2010.04.001.
43. Cipriani E, Bracco P, Kurtz SM, Costa L, Zanetti M. In-vivo degradation of poly(carbonate-urethane) based spine implants. *Polym Degrad Stab*. 2013;98(6):1225–35. DOI: 10.1016/j.polymdegradstab.2013.03.005.

44. Giboz J, Copponnex T, Mélé P. Microinjection molding of thermoplastic polymers: a review. *J Micromechanics Microengineering*. 2007;17(6):R96. DOI: 10.1088/0960-1317/17/6/R02.
45. Rosato DV, Rosato MG. *Injection Molding Handbook*. Springer Science & Business Media; 2012.
46. Chu J, Kamal MR, Derdouri S, Hrymak A. Characterization of the microinjection molding process. *Polym Eng Sci*. 2010;50(6):1214–25. DOI: 10.1002/pen.21632.
47. Smith RA, Hallab NJ. In vitro macrophage response to polyethylene and polycarbonate-urethane particles. *J Biomed Mater Res A*. 2010;93A(1):347–55. DOI: 10.1002/jbm.a.32529.
48. Smith RA, Maghsoodpour A, Hallab NJ. In vivo response to cross-linked polyethylene and polycarbonate-urethane particles. *J Biomed Mater Res A*. 2010;93A(1):227–34. DOI: 10.1002/jbm.a.32531.
49. Khan I, Smith N, Jones E, Finch DS, Cameron RE. Analysis and evaluation of a biomedical polycarbonate urethane tested in an in vitro study and an ovine arthroplasty model. Part II: in vivo investigation. *Biomaterials*. 2005;26(6):633–43. DOI: 10.1016/j.biomaterials.2004.02.064.
50. Angelo Carbone DWH. Aging Performance of a Compliant Layer Bearing Acetabular Prosthesis in an Ovine Hip Arthroplasty Model. *J Arthroplasty*. 2006;21(6):899–906. DOI: 10.1016/j.arth.2005.07.023.
51. Khan I, Smith N, Jones E, Finch DS, Cameron RE. Analysis and evaluation of a biomedical polycarbonate urethane tested in an in vitro study and an ovine arthroplasty model. Part I: materials selection and evaluation. *Biomaterials*. 2005;26(6):621–31. DOI: 10.1016/j.biomaterials.2004.02.065.
52. Smith SL, Ash HE, Unsworth A. A tribological study of UHMWPE acetabular cups and polyurethane compliant layer acetabular cups. *J Biomed Mater Res*. 2000;53(6):710–6. DOI: 10.1002/1097-4636(2000)53:6<710::AID-JBM14>3.0.CO;2-R.

53. Jones E, Scholes SC, Burgess IC, Ash HE, Unsworth A. Compliant layer bearings in artificial joints. Part 2: Simulator and fatigue testing to assess the durability of the interface between an elastomeric layer and a rigid substrate. *Proc Inst Mech Eng [H]*. 2009;223(1):1–13. DOI: 10.1243/09544119JEIM446.
54. Winby CR, Lloyd DG, Besier TF, Kirk TB. Muscle and external load contribution to knee joint contact loads during normal gait. *J Biomech*. 2009;42(14):2294–300. DOI: 10.1016/j.jbiomech.2009.06.019.
55. Huiskes R, Chao EYS. A survey of finite element analysis in orthopedic biomechanics: The first decade. *J Biomech*. 1983;16(6):385–409. DOI: 10.1016/0021-9290(83)90072-6.
56. Büchler P, Ramaniraka NA, Rakotomanana LR, Iannotti JP, Farron A. A finite element model of the shoulder: application to the comparison of normal and osteoarthritic joints. *Clin Biomech*. 2002;17(9–10):630–9. DOI: 10.1016/S0268-0033(02)00106-7.
57. Willing R, Lapner M, Lalone EA, King GJW, Johnson JA. Development of a computational technique to measure cartilage contact area. *J Biomech*. 2014;47(5):1193–7. DOI: 10.1016/j.jbiomech.2014.01.047.
58. Langohr GDG, Willing R, Medley JB, King GJW, Johnson JA. The Effect of Radial Head Hemiarthroplasty Geometry on Proximal Radioulnar Joint Contact Mechanics. *J Hand Surg*. 2016;41(7):745–52. DOI: 10.1016/j.jhsa.2016.05.001.
59. Langohr GDG, Willing R, Medley JB, King GJW, Johnson JA. Contact analysis of the native radiocapitellar joint compared with axisymmetric and nonaxisymmetric radial head hemiarthroplasty. *J Shoulder Elbow Surg*. 2015;24(5):787–95. DOI: 10.1016/j.jse.2014.12.011.
60. Irish SE, Langohr GDG, Willing R, King GJ, Johnson JA. Implications of radial head hemiarthroplasty dish depth on radiocapitellar contact mechanics. *J Hand Surg*. 2015;40(4):723–9. DOI: 10.1016/j.jhsa.2015.01.030.

61. Anderson AE, Ellis BJ, Maas SA, Weiss JA. Effects of idealized joint geometry on finite element predictions of cartilage contact stresses in the hip. *J Biomech.* 2010;43(7):1351–7. DOI: 10.1016/j.jbiomech.2010.01.010.
62. Anderson AE, Ellis BJ, Maas SA, Peters CL, Weiss JA. Validation of Finite Element Predictions of Cartilage Contact Pressure in the Human Hip Joint. *J Biomech Eng.* 2008;130(5):051008–051008. DOI: 10.1115/1.2953472.
63. Bendjaballah M, Shirazi-Adl A, Zukor D. Finite element analysis of human knee joint in varus-valgus. *Clin Biomech.* 1997;12(3):139–48. DOI: 10.1016/S0268-0033(97)00072-7.
64. Li L, Patil S, Steklov N, Bae W, Temple-Wong M, D’Lima DD, et al. Computational wear simulation of patellofemoral articular cartilage during in vitro testing. *J Biomech.* 2011;44(8):1507–13. DOI: 10.1016/j.jbiomech.2011.03.012.
65. Goldsmith AAJ, Hayes A, Clift SE. Application of finite elements to the stress analysis of articular cartilage. *Med Eng Phys.* 1996;18(2):89–98. DOI: 10.1016/1350-4533(95)00029-1.
66. Büchler P, Ramaniraka NA, Rakotomanana LR, Iannotti JP, Farron A. A finite element model of the shoulder: application to the comparison of normal and osteoarthritic joints. *Clin Biomech.* 2002;17(9–10):630–9. DOI: 10.1016/S0268-0033(02)00106-7.
67. Willing RT, Lalone EA, Shannon H, Johnson JA, King GJW. Validation of a finite element model of the human elbow for determining cartilage contact mechanics. *J Biomech.* 2013;46(10):1767–71. DOI: 10.1016/j.jbiomech.2013.04.001.
68. Cilingir AC, Ucar V, Kazan R. Three-dimensional anatomic finite element modelling of hemi-arthroplasty of human hip joint. *Trends Biomater Artif Organs.* 2007.
69. Gabarre S, Herrera A, Mateo J, s, Ibarz E, Lobo-Escolar A, et al. Study of the Polycarbonate-Urethane/Metal Contact in Different Positions during Gait Cycle, Study of the Polycarbonate-Urethane/Metal Contact in Different Positions during Gait Cycle. *BioMed Res Int BioMed Res Int.* 2014:e548968. DOI: 10.1155/2014/548968.

70. Elsner JJ, Portnoy S, Zur G, Guilak F, Shterling A, Linder-Ganz E. Design of a Free-Floating Polycarbonate-Urethane Meniscal Implant Using Finite Element Modeling and Experimental Validation. *J Biomech Eng*. 2010;132(9):095001–095001. DOI: 10.1115/1.4001892.
71. McGann ME, Vahdati A, Wagner DR. Methods to assess in vitro wear of articular cartilage. *Proc Inst Mech Eng [H]*. 2012;226(8):612–22. DOI: 10.1177/0954411912447014.
72. Lizhang J, Taylor SD, Jin Z, Fisher J, Williams S. Effect of clearance on cartilage tribology in hip hemi-arthroplasty. *Proc Inst Mech Eng [H]*. 2013;227(12):1284–91. DOI: 10.1177/0954411913502156.
73. McCann L, Udofia I, Graindorge S, Ingham E, Jin Z, Fisher J. Tribological testing of articular cartilage of the medial compartment of the knee using a friction simulator. *Tribol Int*. 2008;41(11):1126–33. DOI: 10.1016/j.triboint.2008.03.012.
74. Foy JR, Williams PF, Powell GL, Ishihara K, Nakabayashi N, LaBerge M. Effect of phospholipidic boundary lubrication in rigid and compliant hemiarthroplasty models. *Proc Inst Mech Eng [H]*. 1999;213(1):5–18. DOI: 10.1243/0954411991534762.
75. Dalldorf PG, Banas MP, Hicks DG, Pellegrini VD. Rate of degeneration of human acetabular cartilage after hemiarthroplasty. *J Bone Jt Surg Am*. 1995;77(6):877–82.

Chapter 2

Implications of Low Stiffness Biomaterials on Contact Mechanics of Joint Hemiarthroplasty: A Finite Element Study

Overview: *This chapter includes a three-dimensional finite element simulation to investigate the effect of low range implant moduli on implant-cartilage contact area and peak contact stress. A portion of this work was presented at the 2016 Annual Meeting of the Orthopaedic Research Society (Orlando), at the 2016 Canadian Bone & Joint Conference and at the 2016 Annual Meeting of the Canadian Orthopaedic Research Society (Quebec).*

2.1 Introduction

In vitro biomechanical measurement techniques of joint articulations can be difficult to execute and are potentially inaccurate; therefore finite element models are favourable as they are non-invasive alternatives to evaluating contact mechanics¹. Finite element analysis outcomes include contact stress, contact area and stress distributions for intact and replaced joints. The surface of an anatomical (*viz.* bone and cartilage) structure can be discretized and material properties can be assigned to site-specific elements. Contact mechanics at any location within the anatomical structure surface can subsequently be determined, typically at an articulation including an implant if desired.

Finite element simulations have accurately modeled articular cartilage as an anisotropic, biphasic material²⁻⁴. Simpler models have also been successfully reported and are able to reduce the computational expense of the biphasic models. These simpler models use hyperelastic laws and assign a single, non-linear phase to the cartilage⁵⁻⁸. Three-dimensional computed tomography reconstructions are commonly used in finite element applications to account for the elasticity and non-homogenous properties of bone and associated structures such as cartilage by assigning regional properties based on image-based intensity metrics (*i.e.* Hounsfield numbers)^{9,10}.

With respect to examining the effect of implant modulus in hemiarthroplasty systems, only limited studies are available. Johnson et al., assessed the effect of implant modulus in the range of 0.5-230 GPa and showed that the ‘theoretical soft’ material (Young’s modulus of 0.5 GPa) had a significant but small effect on contact area and peak contact stress¹¹. The data suggested that post-operative joint contact mechanics would be optimized if the implant stiffness were reduced even lower than the 0.5 GPa material investigated in the study. Khayat created a two-dimensional axisymmetric finite element model to simulate static pin-on-plate loading for materials with stiffness in the range of ~0.70-200 GPa¹². The results showed no differences in contact stresses among implant materials and suggested a Young’s modulus well below 0.69 GPa may have a more noticeable effect on cartilage contact mechanics.

In view of the foregoing, the objective of the current study was to conduct a three-dimensional finite element simulation to investigate the effect of low range (down to 0.015 GPa) hemiarthroplasty implant moduli on implant-cartilage contact mechanics, with a focus on contact area and contact stress.

2.2 Three-Dimensional Finite Element Modeling

2.2.1 The Model

A three-dimensional model constructed in ABAQUS v6.12-2 (Simula Corp., Providence, RI, USA) as shown in Figure 2-1, was employed. The radius of curvature of the implant was 4.7 mm. The implants were meshed using linear hexahedral elements with an average global edge length of 0.12 mm. The implant consisted of 96,768 linear hexahedral elements, the cartilage layer consisted of 39,896 linear hexahedral elements, and the bone consisted of 265,148 tetrahedral elements. The total degree of freedom for the three dimensional model was therefore 613,695. Peak contact stress and contact area were measured under a constant load of 30 N.

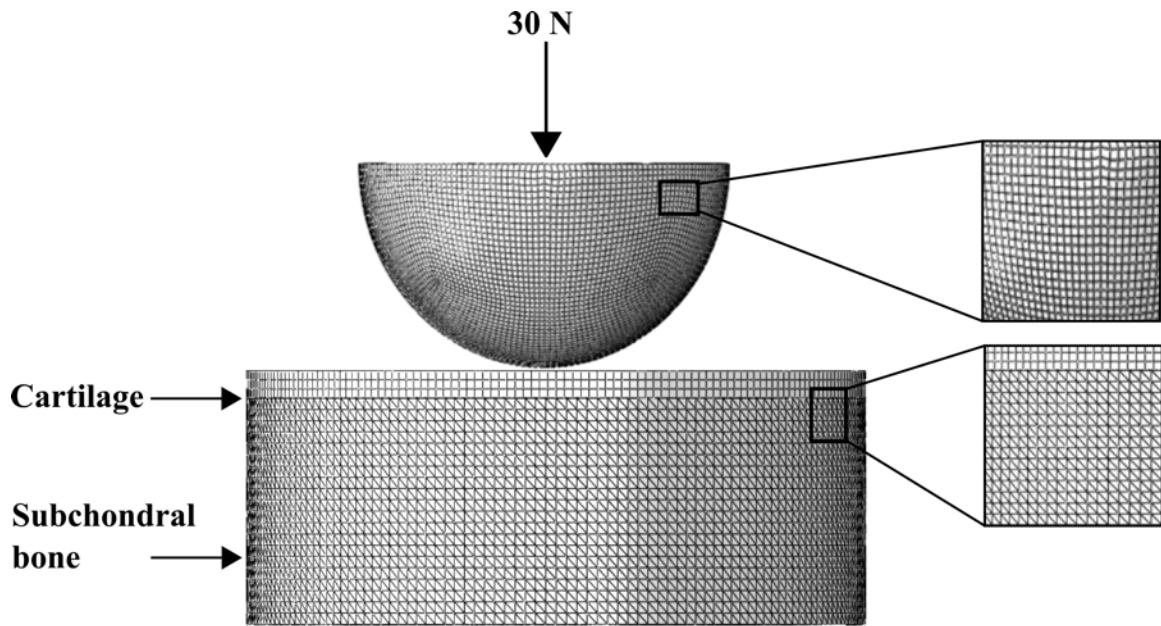


Figure 2-1: Meshes and boundary conditions of the three-dimensional finite element model. All translation and rotation parallel to the cartilage surface were constrained. The pin was constrained in translation perpendicular to the cartilage surface at the guiding node. The subchondral bone guiding node was fully constrained.

The cartilage geometry was assigned a neo-Hookean hyperelastic model in order to simulate the mechanical response cartilage exhibits during equilibrium ($C_{10}= 1.79$)^{5,13}. The cartilage layer was assigned a thickness of 2.5 mm (based on experimental measurements¹²) and consisted of three layers of linear hexahedral mesh with global average edge lengths of 0.15 mm. This type of mesh geometry was used because it allowed the elements to compress without reducing their volume.

The subchondral bone geometry was modeled using an elastic material model and was assigned a Young's modulus of 109 MPa and a Poisson's ratio of 0.3^{14,15}. The bone geometry consisted of tetrahedral mesh elements with edge lengths of 0.1 mm.

All mesh sizes were deemed adequate by mesh convergence studies.

2.2.1.1 Implants

To investigate the effect of material stiffness on contact mechanics, the implants were assigned mechanical properties based on literature values. Bionate-Low was assigned Mooney-Rivlin hyperelastic properties ($C_{10}= 2.912$ and $C_{01}= -1.025$)^{16,17}. Bionate-Mid was modeled elastically with a Young's moduli of 0.039 GPa and Poisson's ratio of 0.45¹⁸. Bionate-High was modeled elastically with a Young's moduli of 0.288 GPa and Poisson's ratio of 0.39¹⁹. Ceramic was modeled elastically with a Young's modulus of 380 GPa and Poisson's ratio of 0.29^{20,21}. Ceramic was chosen to represent a high modulus implant material for comparison.

2.2.1.2 Boundary and Loading Conditions

An assembly was created from the cartilage and subchondral bone models. The two parts were mated using a rigid pin constraint and constrained rotationally and axially. The implant was allowed to move in the plane perpendicular to the cartilage-subchondral bone assembly because the pin was also constrained rotationally and axially. A force of 30 N was applied along the superior-inferior y-axis of the pin model, to press the pin against the cartilage surface to simulate the loading configuration in *in vitro* pin-on-plate wear tests.

2.2.1.3 Outcome Variables

Contact mechanics data was obtained from nodes in the cartilage layer at the implant-cartilage interface. The model output variables were peak contact stress and contact area. The contact area was determined from the region between the nodes where the contact pressure was greater than zero.

2.3 Results

The peak contact stress and contact area determined by the finite element model for the four different Young's moduli values are summarized in Table 2-1. Peak contact stress and contact area are also displayed graphically for the four-implant materials in Figure 2-2. Overall, the data shows peak contact stress increases and contact area decreases as the Young's moduli of the implant material increases. The data also suggests that the response of the three Bionate materials is not linear. Although this cannot be stated without statistical support, it was interesting to note that Bionate-High resulted in contact mechanics that were close to the very stiff ceramic implant modeled, despite a very large difference in modulus (~1300%).

Table 2-1: Summary of FEA results for varying implant moduli

Implant Material	Peak Contact Stress [MPa]	Contact Area [mm ²]
Bionate-Low	4.03	12.71
Bionate-Mid	6.59	8.30
Bionate-High	8.65	6.84
Ceramic	9.27	6.17

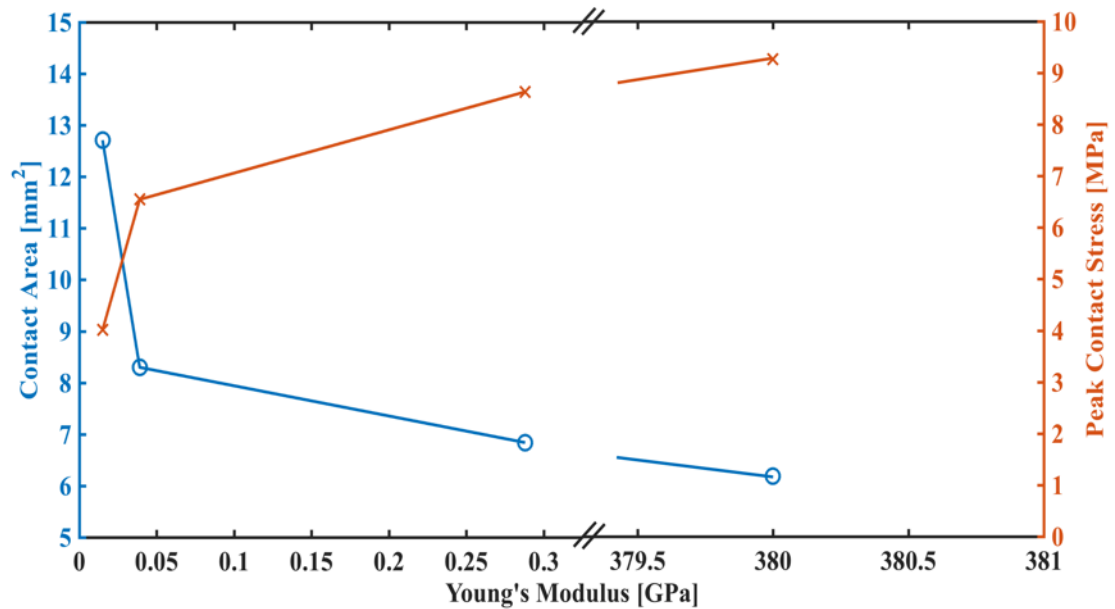
**Figure 2-2: Contact area and peak contact stress for the four implant materials**

Figure 2-3 shows the compressive stress profiles on the cartilage surface for each implant material, which increases as the Young's moduli of the implant increases.

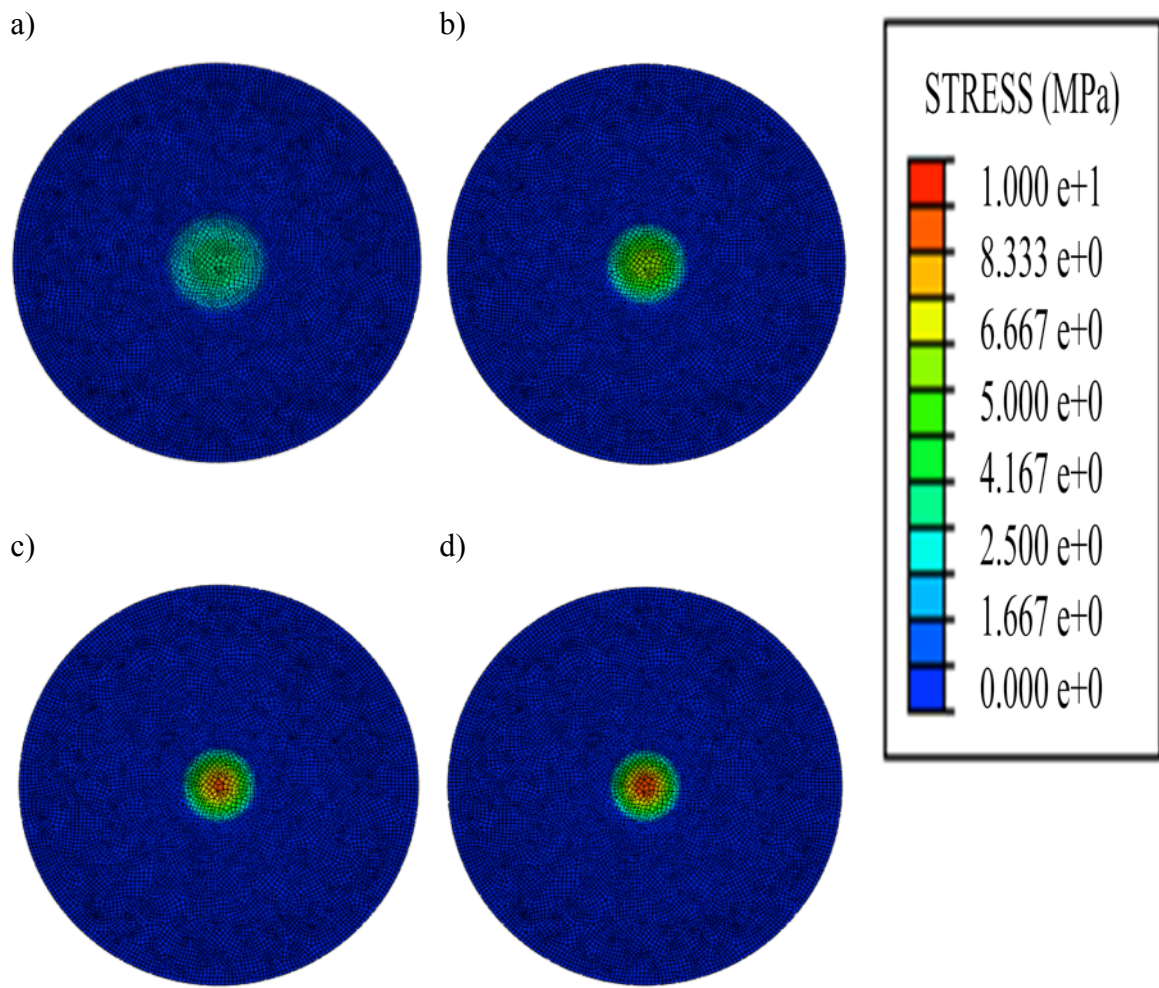


Figure 2-3: Compressive stress profiles on the cartilage surface for various implant models: a) Bionate-Low b) Bionate-Mid c) Bionate-High and d) ceramic

Figure 2-4 shows the contact area between each implant and cartilage, which decreases as the Young's moduli of the implant increases.

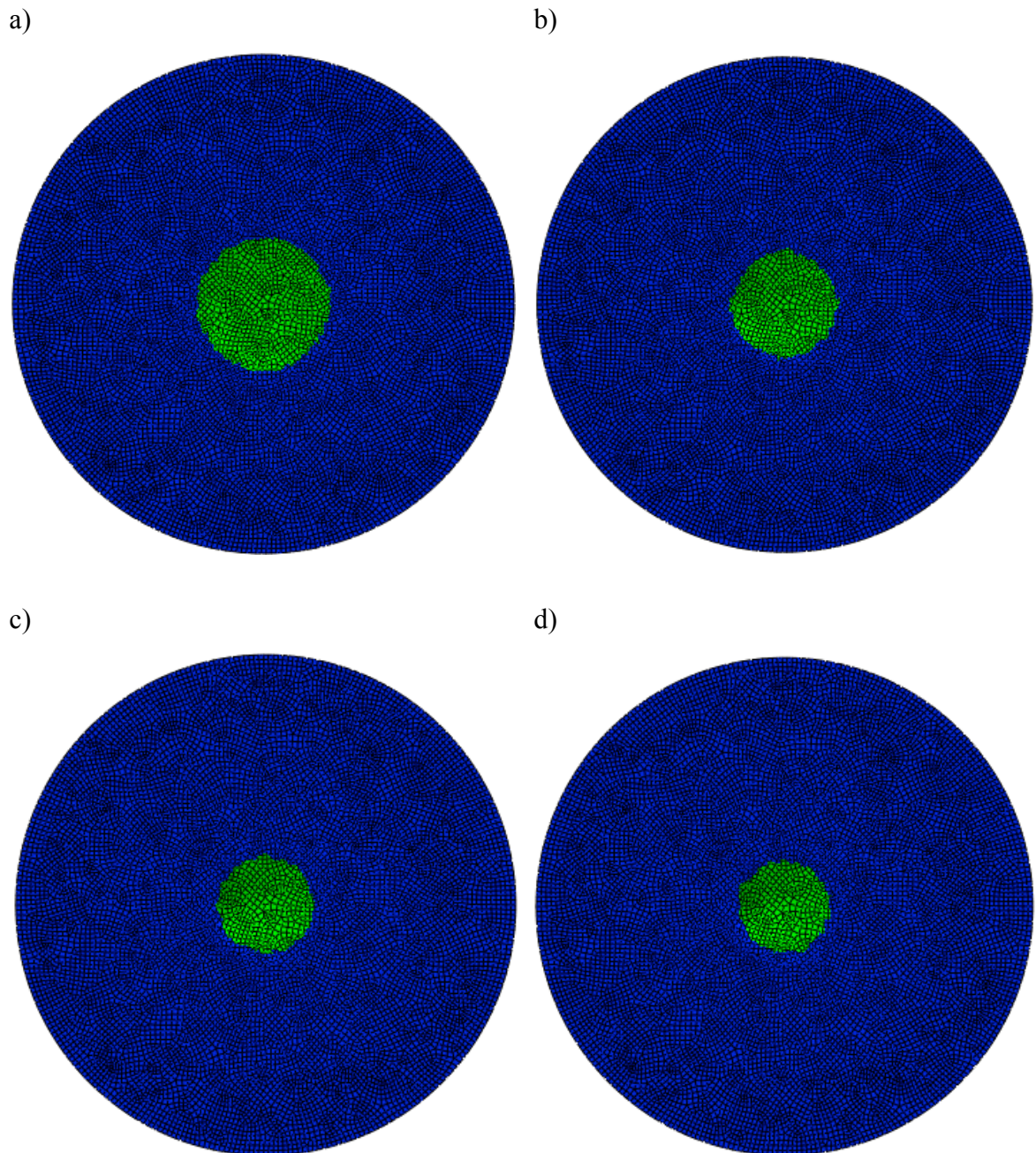


Figure 2-4: Contact areas at the implant-cartilage interface for various implant models: a) Bionate-Low b) Bionate-Mid c) Bionate-High and d) ceramic

Figure 2-5 shows the Von Mises stress distribution at the implant-cartilage interface for each implant material, which increases as the Young's moduli of the implants increases.

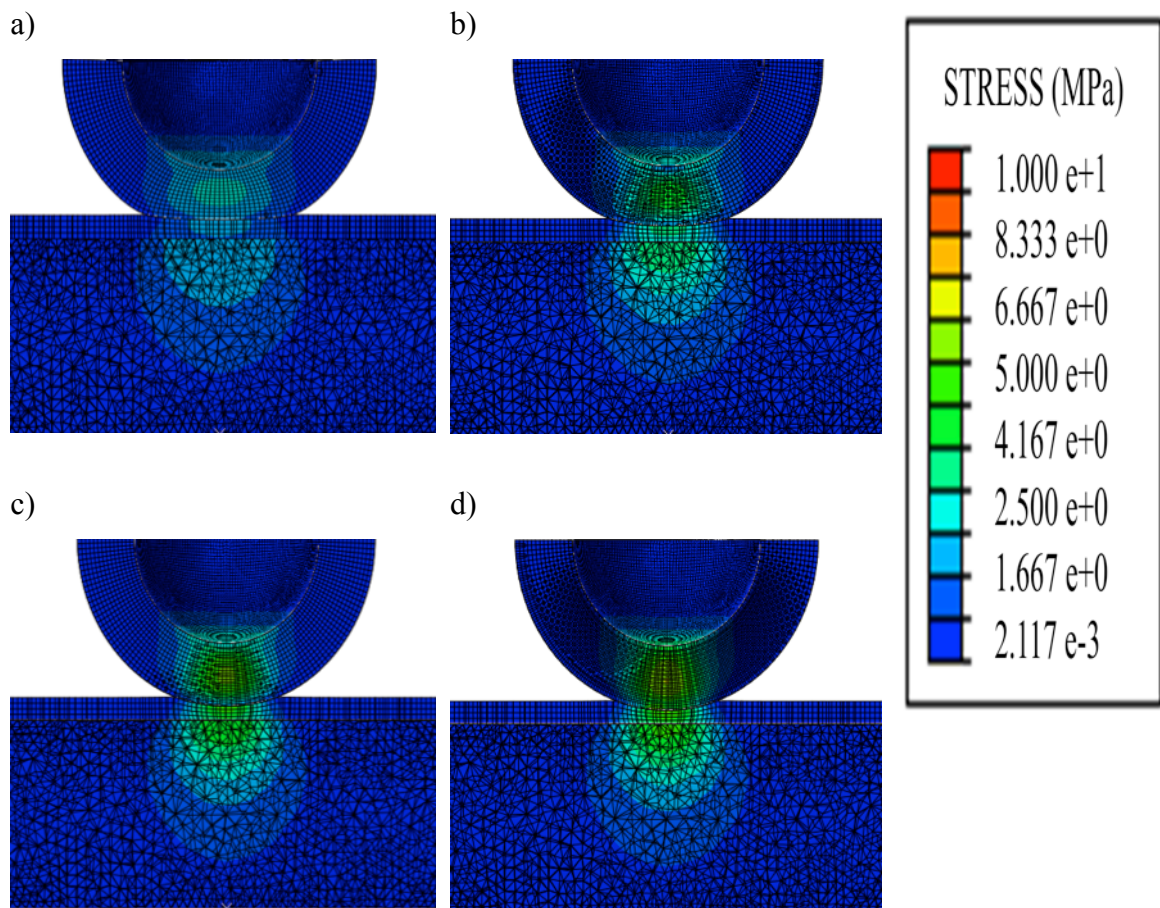


Figure 2-5: Von Mises stress distribution at the implant-cartilage interface for various implant models: a) Bionate-Low b) Bionate-Mid c) Bionate-High and d) ceramic

2.4 Discussion

The study was used to help gain insight into how Bionate interacts with cartilage for hemiarthroplasty applications. Specifically, the effect of low range (down to 0.015 GPa) of hemiarthroplasty implant moduli on contact mechanics using a finite element model was conducted. In general, it was shown that a less stiff material has the ability to deform under compressive forces therefore increasing the contact area and conformity between the implant-cartilage interfaces which results in a decrease in peak contact stress. The findings herein certainly demonstrated these trends. Lower modulus biomaterials have reduced peak contact stress values compared to commonly used implant materials, which suggests that these materials may produce less cartilage degradation²². Decreasing hemiarthroplasty stiffness from 380 to 0.015 GPa increased contact area by 69% and decreased peak contact stress by 79%. When comparing Bionate-Low to Bionate-High, the contact area increases by 60% as the stiffness of the material decreases. Both materials are much softer than currently used implant materials but the results suggest that Bionate-High may not be soft enough to improve contact mechanics. Literature has shown Bionate-Low to have a lower peak contact pressure compared to metal when used as a bearing surface in finite element hip arthroplasty implant models. When compared to a healthy hip joint model, the Bionate-Low had similar peak contact pressures¹⁶. Contact stresses for intact joints have been reported in the range of 0.5 to 6 MPa^{23,24}. Pre-operative and post-operative contact stress has been measured clinically for various hemiarthroplasty procedures (i.e. shoulder, elbow, and hip). Contact stress is increased within the joint after the procedure because the implant reduces the contact area, therefore causing more stress across the articulating surface²⁵⁻²⁸. Thus, this explains why the stress levels in this study were higher than those of native joints.

As regards the modeling employed, there are some limitations. First, creep (time dependent behaviour under compressive loading) of the Bionate was not modeled. Flanagan studied the compressive creep behaviour of Bionate-Low and Bionate-High in *in vitro* conditions for 408 hours²⁹. The study found that there was noticeably less creep resistance in Bionate-Low compared to Bionate-High. Creep deformation increased in both materials as the temperature increased from room temperature to 37°C. Creep

deformation was also compared when the specimens were dry versus lubricated in bovine calf serum. Creep deformation increased with lubrication²⁹. Second, only one implant geometry (i.e. radius of curvature) was modeled. Khayat studied radius of curvatures between 4.7 mm and 11.7 mm in a similar implant finite element study¹². The study showed there is a threshold at which stresses are less sensitive to radius of curvature between the values of 7.25 mm and 9.35 mm. Also, approximations of material properties and behaviour under compressive loading were made. The material properties assigned to the models were taken from literature not directly from experimental measurements. Even though cartilage consists of fluid and solid components, which both distribute loads, this model only accounts for the bulk properties of cartilage and neglects fluid flow through the biphasic poroelastic medium. The FEA model simulated static loading instead of linear reciprocal sliding that will be investigated in the *in vitro* wear study ahead in Chapter 4.

2.5 Conclusion

The decrease in contact stress levels shown by the FEA conducted herein provides insight into the future *in vitro* wear study where a decrease in volumetric wear should be observed as the stiffness of the material decreases. The Bionate-Low model showed the lowest peak contact stress and hence it can be postulated that this material would produce the least amount of cartilage wear. Within the range of implant material moduli examined, a higher contact area and lower peak contact stress were observed as the Young's modulus value decreased which supports that a material with similar characteristics to cartilage improves contact mechanics and should decrease cartilage wear. The experimental performance of these different Bionate formulations is provided in Chapter 4.

2.6 References

1. Winby CR, Lloyd DG, Besier TF, Kirk TB. Muscle and external load contribution to knee joint contact loads during normal gait. *J Biomech.* 2009;42(14):2294–300. DOI: 10.1016/j.jbiomech.2009.06.019.
2. Goldsmith AAJ, Hayes A, Clift SE. Application of finite elements to the stress analysis of articular cartilage. *Med Eng Phys.* 1996;18(2):89–98. DOI: 10.1016/1350-4533(95)00029-1.
3. Clift SE. Annual Scientific Meeting Finite-element analysis in cartilage biomechanics. *J Biomed Eng.* 1992;14(3):217–21. DOI: 10.1016/0141-5425(92)90055-P.
4. Huiskes R, Chao EYS. A survey of finite element analysis in orthopedic biomechanics: The first decade. *J Biomech.* 1983;16(6):385–409. DOI: 10.1016/0021-9290(83)90072-6.
5. Büchler P, Ramaniraka NA, Rakotomanana LR, Iannotti JP, Farron A. A finite element model of the shoulder: application to the comparison of normal and osteoarthritic joints. *Clin Biomech.* 2002;17(9–10):630–9. DOI: 10.1016/S0268-0033(02)00106-7.
6. Anderson AE, Ellis BJ, Maas SA, Weiss JA. Effects of idealized joint geometry on finite element predictions of cartilage contact stresses in the hip. *J Biomech.* 2010;43(7):1351–7. DOI: 10.1016/j.jbiomech.2010.01.010.
7. Anderson AE, Ellis BJ, Maas SA, Peters CL, Weiss JA. Validation of Finite Element Predictions of Cartilage Contact Pressure in the Human Hip Joint. *J Biomech Eng.* 2008;130(5):051008–051008. DOI: 10.1115/1.2953472.
8. Willing RT, Lalone EA, Shannon H, Johnson JA, King GJW. Validation of a finite element model of the human elbow for determining cartilage contact mechanics. *J Biomech.* 2013;46(10):1767–71. DOI: 10.1016/j.jbiomech.2013.04.001.

9. Pauwels R, Jacobs R, Singer SR, Mupparapu M. CBCT-based bone quality assessment: are Hounsfield units applicable? *Dento Maxillo Facial Radiol.* 2015;44(1):20140238. DOI: 10.1259/dmfr.20140238.
10. Schreiber JJ, Anderson PA, Rosas HG, Buchholz AL, Au AG. Hounsfield Units for Assessing Bone Mineral Density and Strength: A Tool for Osteoporosis Management. *J Bone Jt Surg.* 2011;93(11):1057–63. DOI: 10.2106/JBJS.J.00160.
11. Johnson A, Langohr DG, King GJW, Johnson JA. The Effect of Radial Head Hemiarthroplasty Stiffness on Joint Contact Mechanics. 2015.
12. Khayat A. Effect of Hemiarthroplasty Implant Contact Geometry and Material on Early Cartilage Wear. *Electron Thesis Diss Repos.* 2015.
13. Büchler P, Farron A. Benefits of an anatomical reconstruction of the humeral head during shoulder arthroplasty: a finite element analysis. *Clin Biomech.* 2004;19(1):16–23. DOI: 10.1016/j.clinbiomech.2003.09.009.
14. Wirtz DC, Schiffers N, Pandorf T, Radermacher K, Weichert D, Forst R. Critical evaluation of known bone material properties to realize anisotropic FE-simulation of the proximal femur. *J Biomech.* 2000;33(10):1325–30. DOI: 10.1016/S0021-9290(00)00069-5.
15. Mow VC, Hayes WC. *Basic Orthopaedic Biomechanics.* Raven Press; 1991.
16. Gabarre S, Herrera A, Mateo J, s, Ibarz E, Lobo-Escolar A, et al. Study of the Polycarbonate-Urethane/Metal Contact in Different Positions during Gait Cycle, Study of the Polycarbonate-Urethane/Metal Contact in Different Positions during Gait Cycle. *BioMed Res Int BioMed Res Int.* 2014;2014, 2014:e548968. DOI: 10.1155/2014/548968.
17. Elsner JJ, Portnoy S, Zur G, Guilak F, Shterling A, Linder-Ganz E. Design of a Free-Floating Polycarbonate-Urethane Meniscal Implant Using Finite Element Modeling and Experimental Validation. *J Biomech Eng.* 2010;132(9):095001–095001. DOI: 10.1115/1.4001892.

18. Simmons A, Hyvarinen J, Odell RA, Martin DJ, Gunatillake PA, Noble KR, et al. Long-term in vivo biostability of poly(dimethylsiloxane)/poly(hexamethylene oxide) mixed macrodiol-based polyurethane elastomers. *Biomaterials*. 2004;25(20):4887–900. DOI: 10.1016/j.biomaterials.2004.01.004.
19. Ghail NNA, Little EG. Determination of the mechanical properties of Bionate 80A and Bionate 75D for the stress analysis of cushion form bearings. *Proc Inst Mech Eng [H]*. 2008;222(5):683–94. DOI: 10.1243/09544119JEIM372.
20. Paipetis AS, Matikas TE, Aggelis DG, Hemelrijck DV. *Emerging Technologies in Non-Destructive Testing V*. CRC Press; 2012.
21. Valet S, Weisse B, Kuebler J, Zimmermann M, Affolter C, Terrasi GP. Are asymmetric metal markings on the cone surface of ceramic femoral heads an indication of entrapped debris? *Biomed Eng OnLine*. 2014;13:38. DOI: 10.1186/1475-925X-13-38.
22. McGibbon CA, Krebs DE, Trahan CA, Trippel SB, Mann RW. Cartilage degeneration in relation to repetitive pressure: Case study of a unilateral hip hemiarthroplasty patient. *J Arthroplasty*. 1999;14(1):52–8. DOI: 10.1016/S0883-5403(99)90202-4.
23. Brand RA. Joint Contact Stress. *Iowa Orthop J*. 2005;25:82–94.
24. Park S, Hung CT, Ateshian GA. Mechanical response of bovine articular cartilage under dynamic unconfined compression loading at physiological stress levels. *Osteoarthritis Cartilage*. 2004;12(1):65–73. DOI: 10.1016/j.joca.2003.08.005.
25. Petraglia CA, Ramirez MA, Tsai MA, Parks BG, Murthi AM. Glenohumeral Pressure With Surface Replacement Arthroplasty Versus Hemiarthroplasty. *Orthopedics*. 2014;37(10):e892–6. DOI: 10.3928/01477447-20140924-55.
26. Genda E, Iwasaki N, Li G, MacWilliams BA, Barrance PJ, Chao EYS. Normal hip joint contact pressure distribution in single-leg standing—effect of gender and anatomic parameters. *J Biomech*. 2001;34(7):895–905. DOI: 10.1016/S0021-9290(01)00041-0.

27. Hodge WA, Fijan RS, Carlson KL, Burgess RG, Harris WH, Mann RW. Contact pressures in the human hip joint measured in vivo. *Proc Natl Acad Sci U S A*. 1986;83(9):2879–83.
28. Sahu D, Holmes DM, Fitzsimmons JS, Thoreson AR, Berglund LJ, An K-N, et al. Influence of radial head prosthetic design on radiocapitellar joint contact mechanics. *J Shoulder Elb Surg Am Shoulder Elb Surg Al*. 2014;23(4):456–62. DOI: 10.1016/j.jse.2013.11.028.
29. Flanagan S. *Friction, Lubrication and Wear of Total Joint Replacements*. University of Limerick, 2010.

Chapter 3

Fabrication and Characterization of Bionate Implants

Overview: This chapter describes the fabrication of Bionate-Low, Bionate-Mid and Bionate-High implants using microinjection moulding. TGA, DSC and compressive load testing characterized the chemical and mechanical properties of the implants.

3.1 Introduction

As previously discussed in Chapter 1 (Section 1.4.3), injection moulding has been used to mould Bionate for several total arthroplasty applications. The injection moulding process involves four stages: plasticization, clamping, moulding-holding, and demoulding¹. The process melts polymer pellets and then the mould is pressed together to allow the melted polymer to be injected into a mould cavity (the desired mould shape). The polymer is given time to cool before the moulded part is released. Bionate implants have been created with a Bionate 75D (Bionate-High) backing and then over moulded with a Bionate 80A (Bionate-Low) articulating layer for hip acetabular cups², shoulder glenoid components^{3,4}, and knee tibial bearing inserts⁵. A newer type of injection moulding that has been established is microinjection moulding. Microinjection moulding is a more efficient process for large-scale fabrication and is used to produce thermoplastic polymer micro-components for biomedical, electronic, and microelectromechanical systems^{1,6}.

Chemical analysis is performed on materials to determine chemical properties such as thermal stability, phase change, water absorption, and glass transition temperature. Two commonly used techniques to characterize chemical properties of a material are thermogravimetric analysis (TGA) and differential scanning calorimetry (DSC). TGA is used to measure the change in mass of the polymer as the temperature is increased. It gives insight into when decomposition of the material occurs. DSC determines the change in the amount of heat required to increase the temperature of a material. This technique is used to determine physical transformation of the polymer. For example, glass transition temperature, phase change and melting of crystalline regions can be determined using DSC⁷.

Mechanical testing is performed on materials to determine mechanical properties such as elasticity (Young's modulus), elongation, fatigue limit, fracture toughness, and tensile strength. Mechanical properties of interest for joint replacements are Young's modulus and strength^{7,8}. The manufacturer of Bionate, DSM Biomedical, has previously measured the hardness of this material. ASTM D2240 durometers are used to measure the hardness of Bionate and classify the material into two scales, Shore A and Shore D scale⁹. The durometer applies a given force to the material and measures the depth of indentation. Both scales result in a value between 0 and 100, where higher numbers indicate a harder material. The A scale is used for softer plastics, while the D scale is used for harder plastics. Bionate-Low is categorized by the A scale with a value of 80A. Bionate-Mid and Bionate-High are categorized by the D scale with values of 55D and 75D, respectively. Ghail et al., used cyclic volumetric compression testing at 37.5°C and 0.5 mm/min to determine the Young's moduli of Bionate-Low and Bionate-High⁸. The mean Young's modulus of Bionate-Low over 10 loading cycles was 23.24 MPa. The mean Young's modulus of Bionate-High over 10 loading cycles was 271.5 MPa.

The purpose of the present study was to fabricate Bionate implants using microinjection moulding. After the implants were fabricated, they were characterized by TGA, DSC, and Instron compressive loading to evaluate chemical and mechanical properties of Bionate.

3.2 Materials and Methods

3.2.1 Bionate Drying Conditions

The raw Bionate pellets (DSM Biomedical, California, USA) were dried in a vacuum oven (OV-11 Vacuum Oven, Jeiotech) at 90°C for 5 hours. After being dried, the pellets were placed in glass desiccators with indicating silica gel to sustain the dry state of the pellets until they were moulded into Bionate implants.

3.2.2 Microinjection Moulding Conditions

The Bionate pellets were subjected to microinjection moulding in a Battenfeld Microsystem 50 (Wittmann Battenfeld GmbH, Austria). The mould insert was manufactured at University Machine Services at the University of Western Ontario. The

cavity plate of the mould insert can be seen in Figure 3-1. The mould was made from 6061 aluminum and P20 tool steel. The tool steel was used in high wear locations because it is pre-hardened and allows for better surface finish on polished surfaces. The hemispherical cavities were the only component of the mould that was polished to reduce tooling marks on the surface being transferred to pin. Due to the maximum amount of material that could be injected, the mould could eject two pins per injection. Each pin had an approximate volume of 0.4 cm^3 with radius of curvature of 4.7 mm, diameter of 9.4 mm and height of 1 cm. A schematic of the pin moulded from Bionate pellets can be seen in Figure 3-1.

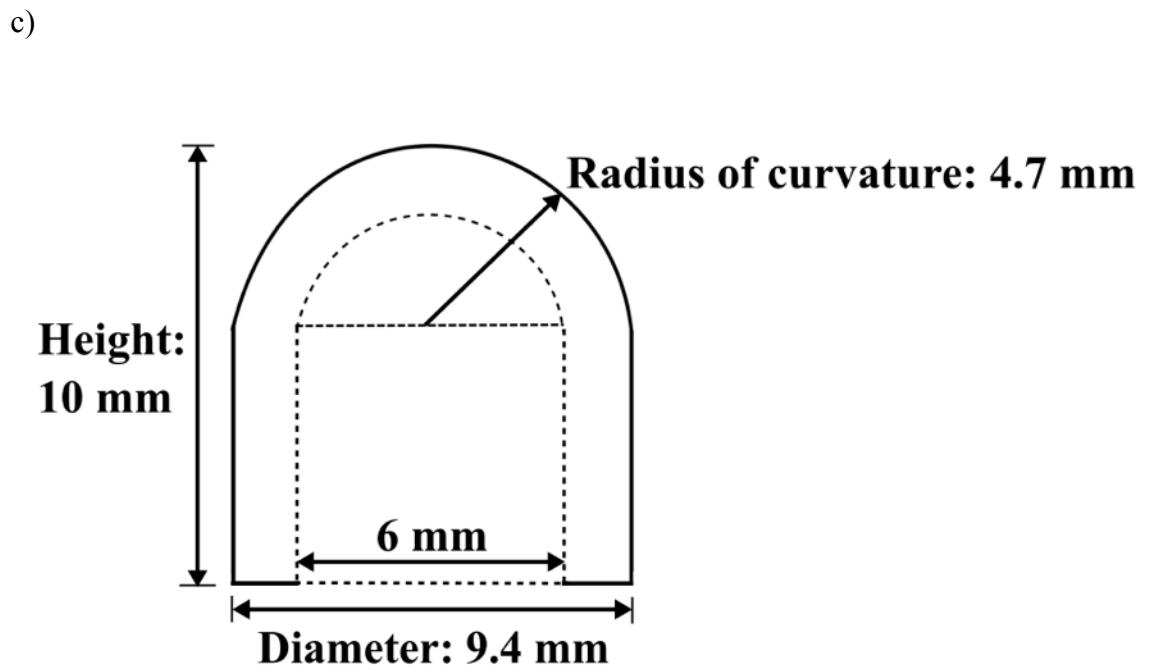
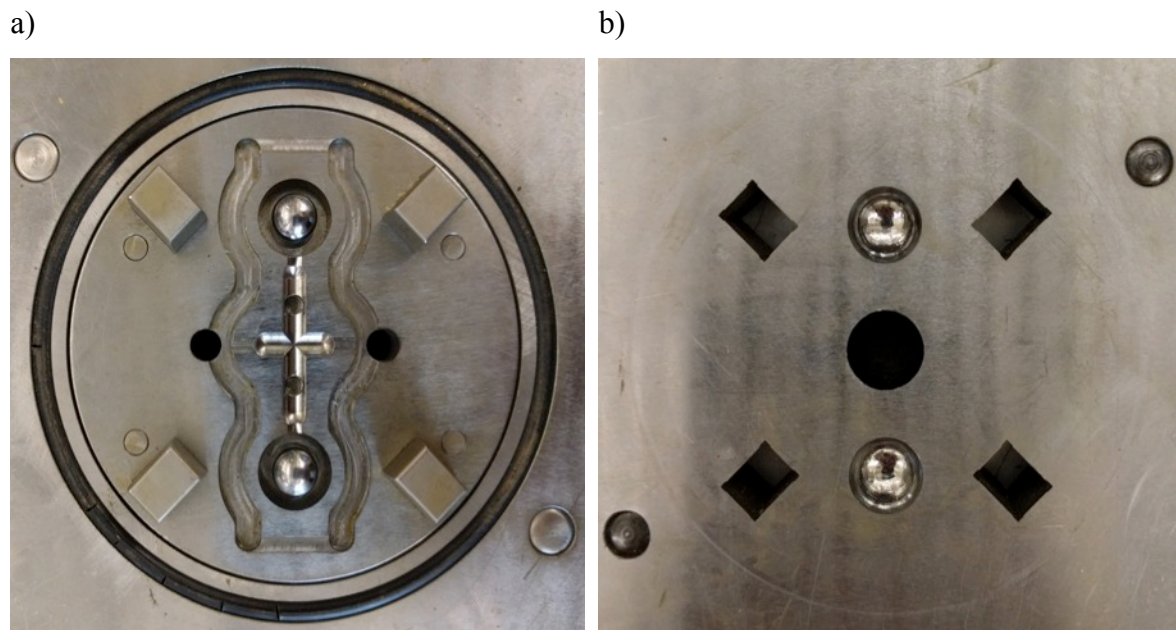


Figure 3-1: a) Image of the cavity plate of the mould insert b) image of the other side of the mould insert c) schematic of final moulded Bionate pin

The same operating conditions were used to mould all three grades of Bionate and are listed in Table 3-1. The dried Bionate pellets were placed into the Battenfeld hopper. Only one grade of Bionate was processed at a time to avoid cross contamination between polymers. A medical-grade lubricant called Pure Eze Mold Release was sprayed on the ejection side of the mould to improve pin release. The microinjection moulding process is represented in a schematic seen in Figure 3-2.

Table 3-1: Battenfeld Microsystem 50 operating conditions

Nozzle temperature (°C)	200
Melt temperature (°C)	200
Mould temperature (°C)	40
Cooling time (s)	20
Clamping force (kN)	50
Holding pressure (bar)	1000
Injection pressure (bar)	2500
Injection speed (mm/s)	760
Injection volume (mm ³)	1100

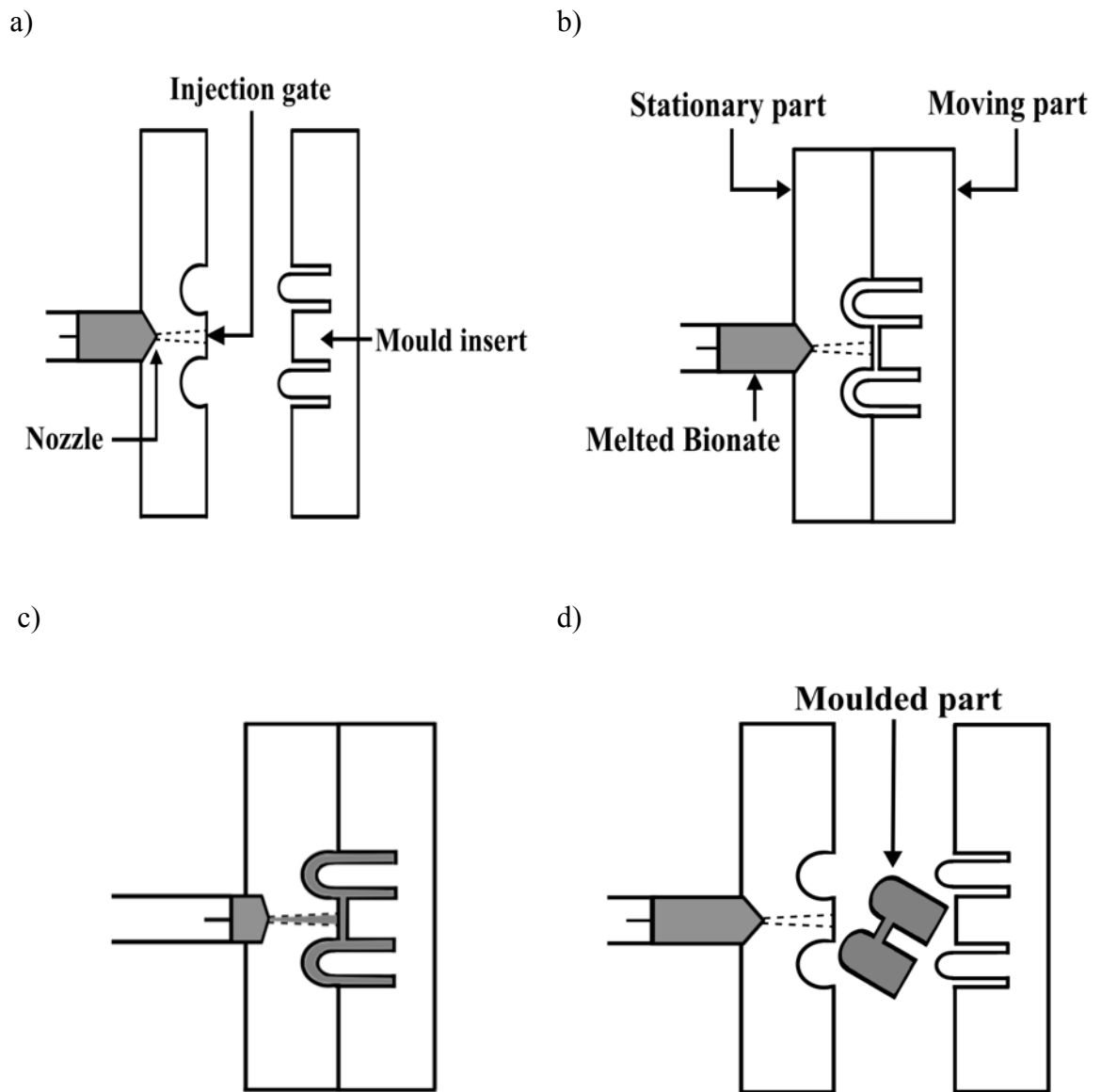


Figure 3-2: Schematic drawing of the microinjection moulding process: a) plasticization b) clamping c) moulding-holding and d) demoulding

3.3 Thermal Analysis of Bionate

3.3.1 Materials and Methods

3.3.1.1 Thermogravimetric Analysis (TGA)

The thermal stability of Bionate-Low, Bionate-Mid, and Bionate-High were measured using a Mettler Toledo TGA/SDTA851e model (Mettler-Toledo Inc., Mississauga, ON, Canada). An 11 mg pellet sample was contained in an aluminum pan. The sample was heated from 25°C up to 600°C with a heating ramp of 10°C/min under nitrogen purge of 40 mL/min.

3.3.1.2 Differential Scanning Calorimetry (DSC)

A differential scanning calorimeter (DSC822e, Mettler Toledo Inc., Mississauga, ON, Canada) was used to determine physical transformations of Bionate-Low, Bionate-Mid, and Bionate-High. A 4 mg pellet sample was contained in an aluminum pan with a 10°C/min heating ramp from -75°C up to 200°C under nitrogen atmosphere.

3.3.2 Results

3.3.2.1 Thermogravimetric Analysis

The TGA results shown in Figure 3-3 display the change in mass for each grade of Bionate. The curves displayed in Figure 3-4 show the rate of mass change over time for each grade of Bionate. Bionate-Low and Bionate-Mid start to decompose around the same temperature and Bionate-Low has the highest temperature of maximal rate of mass loss.

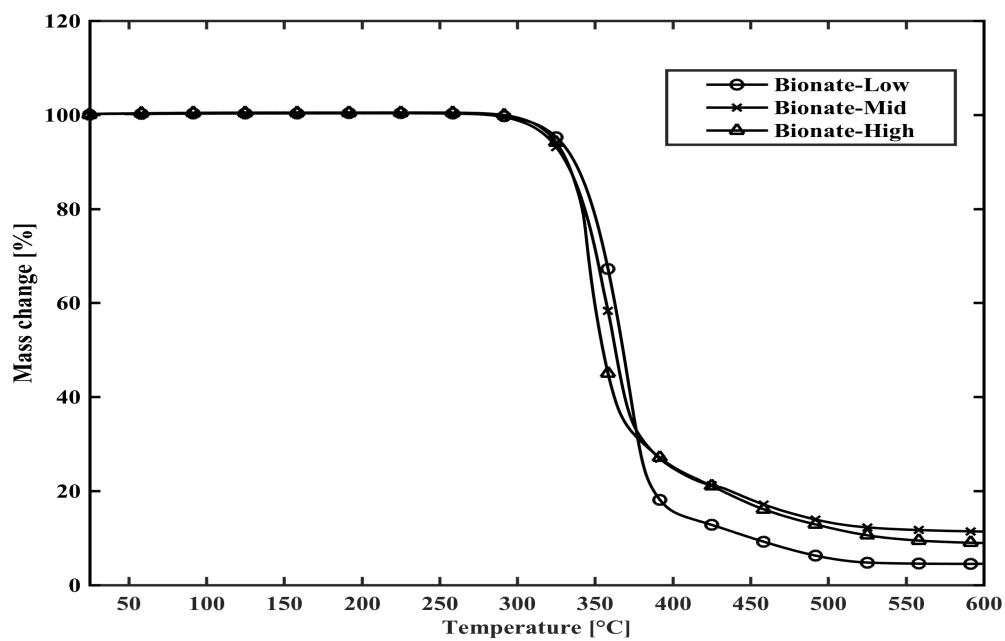


Figure 3-3: TGA mass change curves for Bionate-Low, Bionate-Mid and Bionate-High

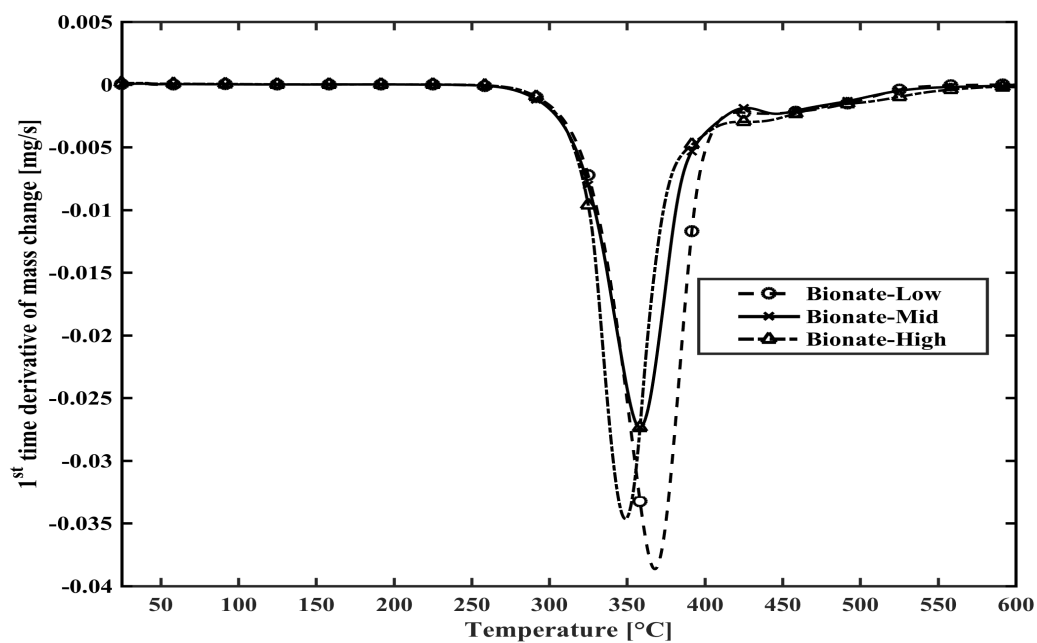


Figure 3-4: TGA first derivative of mass change curve for Bionate-Low, Bionate-Mid and Bionate-High

3.3.2.2 Differential Scanning Calorimetry

The DSC results shown in Figure 3-5 display the crystallization process of Bionate-Low, Bionate-Mid and Bionate-High up to 200°C (this temperature was selected because thermal degradation of Bionate occurs between 210-230°C).

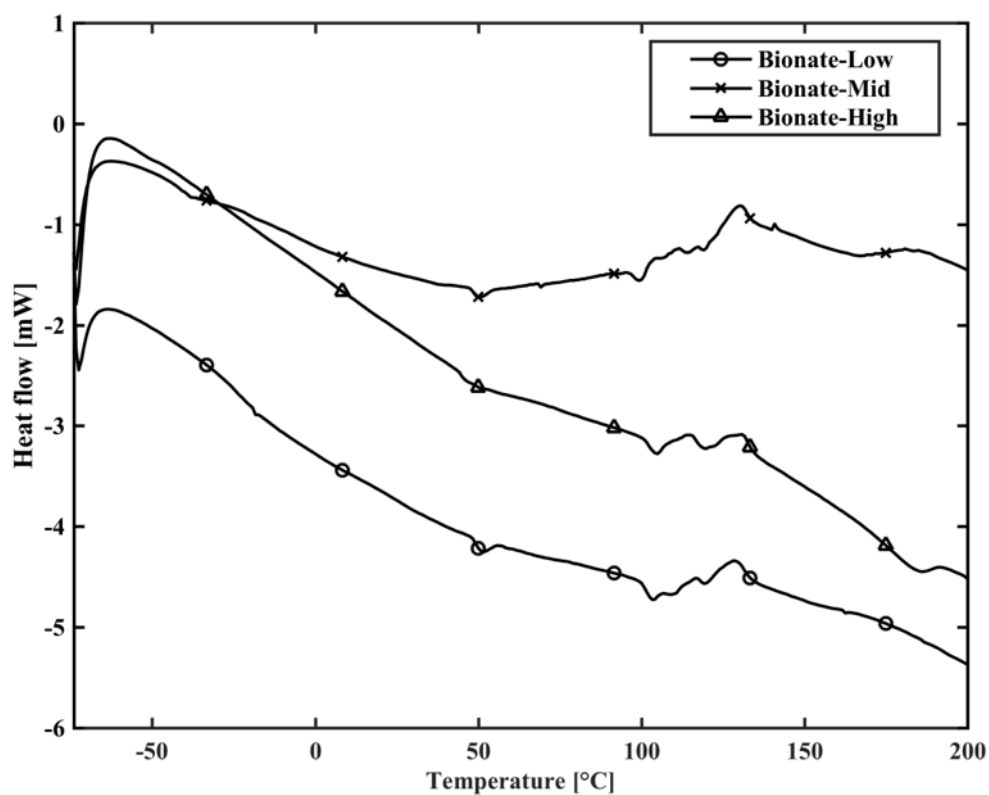


Figure 3-5: DSC analysis of Bionate-Low, Bionate-Mid and Bionate-High

3.3.3 Discussion

3.3.3.1 Thermogravimetric Analysis

The peak of the first derivative curve indicates the point where the largest rate of change on the mass loss curve occurs. The minimum point on the peak is the temperature of maximal rate of mass loss and is called the point of inflection. The point of inflection for Bionate-Low, Bionate-Mid, and Bionate-High occurred at 369.00°C, 359.67°C and 349.00°C, respectively. The effect of heat on the polymer chain is believed to take place on the urethane bonds. The phenomenon that is occurring is called transurethanization (urethane bonds dissociate and re-associate simultaneously). At high temperatures where the urethane bonds are no longer stable, equilibrium shift within the polymer moves towards dissociation of urethane bonds and volatile low molecular mass fragments are the main product¹⁰. Since Bionate consists of hard and soft segments, the hard-to-soft segment ratio can be used to better explain the inflection points. Higher thermal and mechanical properties occur in polycarbonate urethane polymers when there is a higher hard-to-soft segment ratio¹¹. Bionate is composed of a hard segment (polyurethane) and a soft segment (polycarbonate). The hard segment of the polymer determines the stiffness of the polymer and therefore the more polyurethane in the polymer, the higher the polymer stiffness¹². As determined in another study³ and from the mechanical assessment covered later in this chapter, Bionate-High has the highest stiffness out of the three different grades of Bionate that were studied. Bionate-High had more urethane bonds, which means more urethane bonds were ruptured as the temperature increased in the TGA. Decrease in inflection point temperature as the hard segment content increased in polycarbonate urethane has been documented in literature¹³.

From the TGA data, mass loss for Bionate-Low, -Mid and -High were determined. Mass loss was calculated by the following equation (Equation 3-1):

$$\mathbf{Mass\ loss} = \left| \left(\frac{\mathbf{Final\ mass} - \mathbf{Initial\ mass}}{\mathbf{Initial\ mass}} \right) \right| \times \mathbf{100\%} \quad \mathbf{(3-1)}$$

The initial mass (mg) is determined by the value where sample decomposition starts and the final mass (mg) is determined by the value where sample decomposition ends. As

shown in Table 3-2, thermal decomposition started to occur in Bionate-Low, -Mid, and -High at 210.33°C, 209.00°C, and 227.00°C, respectively. All three-onset temperatures are not far from the suggested processing conditions¹⁴. Bionate-Low is suggested to be processed between 190-210°C, while Bionate-Mid and -High are suggested to be processed between 200-210°C.

As shown in Table 3-2, 95.51% mass loss occurred during decomposition between 210.33 and 583.67°C for Bionate-Low. 88.57% mass loss occurred between 209.00 and 583.67°C for Bionate-Mid. 90.97% mass loss occurred between 227.00 and 583.67°C for Bionate-High. Bionate-High starts to decompose at a higher temperature than Bionate-Low and -Mid, but exhibits a faster rate of decomposition.

Table 3-2: TGA data of Bionate-Low, Bionate-Mid and Bionate-High

Bionate Grade	Start of Decomposition (°C)	Point of Inflection (°C)	End of Decomposition (°C)	Mass Loss (%)
Low	210.33	369.00	583.67	95.51
Mid	209.00	359.67	583.67	88.57
High	227.00	349.00	583.67	90.97

3.3.3.2 Differential Scanning Calorimetry

Some polycarbonate urethanes exhibit two glass transition temperatures due to their copolymer nature. A glass transition temperature is associated with the soft segment of the polymer and occurs in the range of -40°C to -20°C¹³. The second glass transition temperature is associated with the hard segment of the polymer and occurs above 0°C¹³. Bionate has been reported to only have one glass transition temperature because the amorphous segment is small. Geary et al.³, determined the glass transition temperatures for Bionate 80A and 75D and there was no evidence of two-phase behaviour. The glass

transition temperatures of Bionate 80A and 75D have been determined to occur at 17°C and 76°C, respectively³. Another study determined the glass transition temperature of Bionate 80A at -16.2°C⁷.

The glass transition occurs when the amorphous material transitions from a brittle glassy state into rubber like molten state as the temperature increases. The glass transition temperature will always be lower than the melting temperature of the crystalline state. The DSC results for glass transition temperature and start of crystallization melting are shown in Table 3-3. Endothermic signals are present for each grade of Bionate ranging from 100°C to 130°C. These endothermic peaks are associated with the disordering of hard micro-domains and strongly related to the thermal history of the Bionate samples¹⁰.

Table 3-3: DSC data of Bionate-Low, Bionate Mid and Bionate-High

Bionate Grade	Glass Transition Temperature (°C)	Start of Crystallization Melting (°C)
Low	-23.0	126.67
Mid	-10.0	134.17
High	27.5	120.83

3.4 Mechanical Properties of Bionate

3.4.1 Materials and Methods

To determine the Young's modulus of each implant material, axial compressive loading was applied to each implant type using an Instron 8500 (Norwood, MA, USA). The hemispherical tip of each implant was removed leaving a hollow cylinder (5 mm in height) to be used for compressive loading. Three specimens of each material were tested. The hollow cylinder was placed into the Instron machine and an initial force was applied to the cylinder. The initial deformation length was determined (Figure 3-6). The change in force (ΔF) and change in deformation length (ΔL) were measured throughout

compressive loading. For Bionate-Low and Bionate-Mid (n=3), the applied force of the cylinder was determined at increments of 0.1 mm (deformation length) from 0 mm to 1 mm. For Bionate-High (n=3), the applied force was determined at increments of 0.05 mm from 0 mm to 0.5 mm.

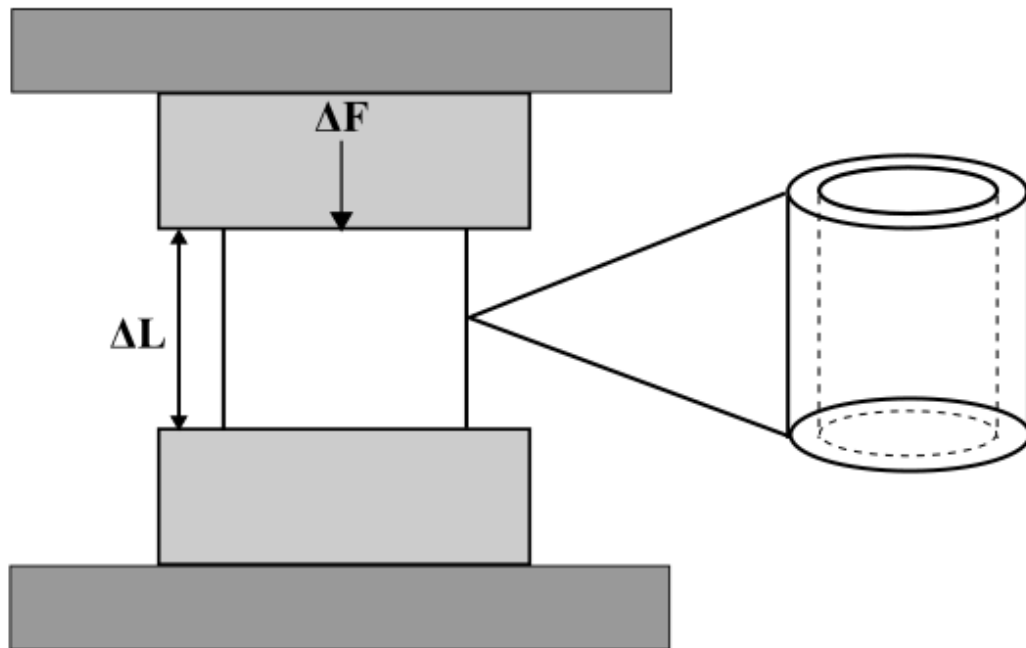


Figure 3-6: Schematic of Bionate implant under compressive loading within the Instron

3.4.2 Results

The compression stress-strain results for each grade of Bionate are presented in Figure 3-7.

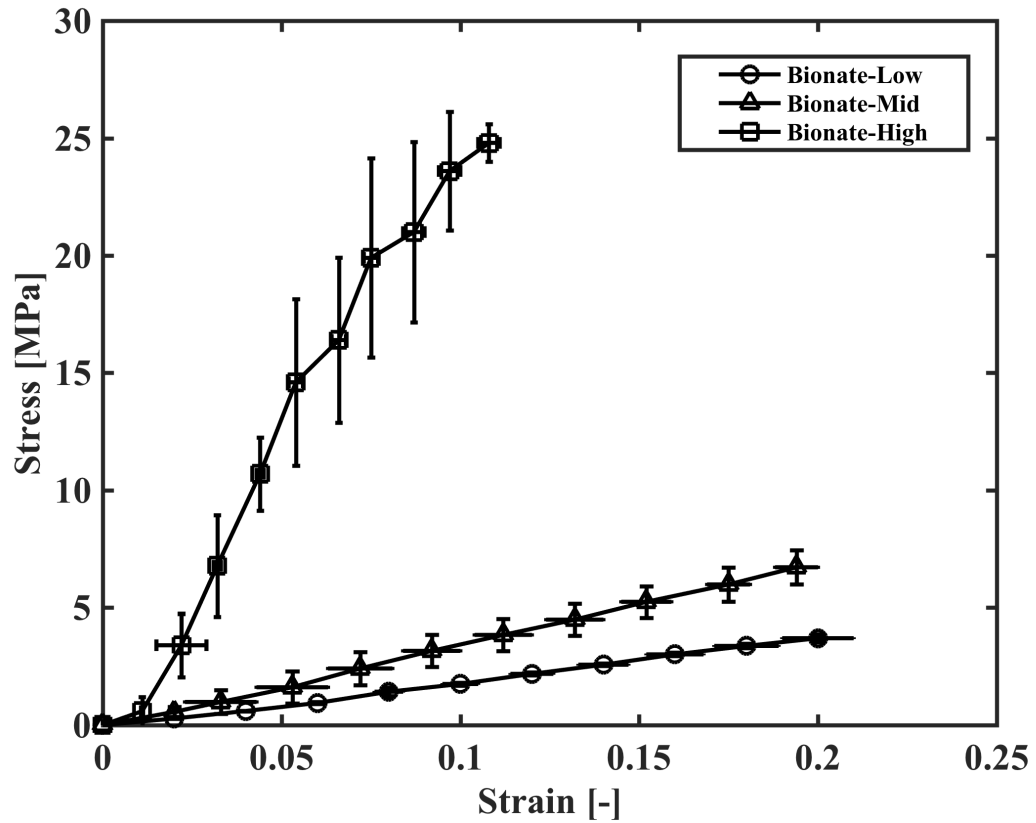


Figure 3-7: Mean (\pm one standard deviation) stress-strain curve for all three grades of Bionate

The Young's modulus was determined from the calculated axial stress (σ) and strain (ε) for each material (refer to Equation 3-2).

$$E = \frac{\sigma}{\varepsilon} \quad (3-2)$$

Axial stress was calculated by:

$$\sigma = \frac{F}{A} \quad (3-3)$$

σ is the axial stress [MPa], F is the compressive load [N] and A is the cross sectional area of the hollow cylinder [mm²].

Axial strain was calculated by:

$$\varepsilon = \frac{\Delta L}{L_{initial}} \quad (3-4)$$

ε is the axial strain, ΔL is change in deformation length [mm] and $L_{initial}$ is initial deformation length before compressive loading begins [mm]. From the stress-strain curves, the Young's moduli of Bionate-Low, -Mid and -High were determined and are displayed graphically as the mean (n=3) \pm standard deviation in Figure 3-8.

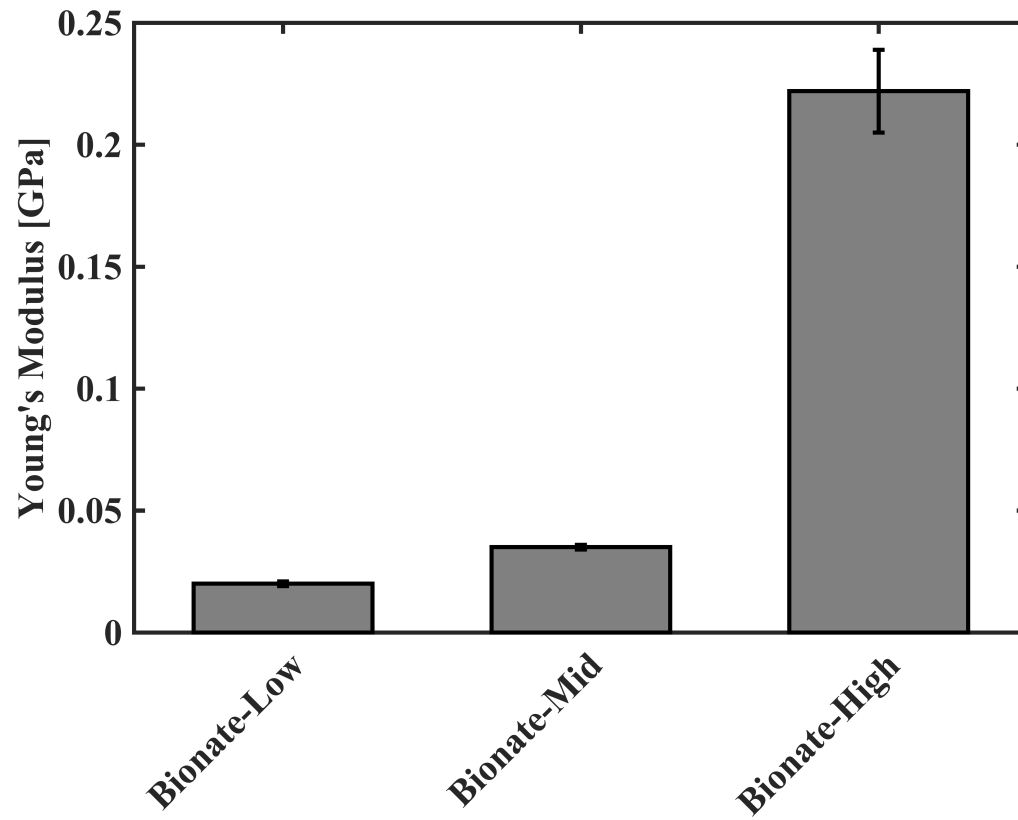


Figure 3-8: Mean (\pm one standard deviation) Young's moduli for Bionate-Low, Bionate-Mid and Bionate-High

3.4.3 Discussion

The data demonstrates the mechanical differences that occur between the different Bionate formulations. The mean Young's moduli (\pm one standard deviation) for Bionate-Low, -Mid, and -High were 0.020 ± 0.001 GPa, 0.035 ± 0.001 GPa, and 0.222 ± 0.017 GPa, respectively. The larger standard deviation value for Bionate-High was attributed to one of the specimens reached high forces quite quickly and another specimen failed at deformation length of 0.4 mm. The calculated Young's moduli values agree to values reported in literature^{8,15}. This data would seem to suggest that the wear characteristics of Bionate-Low and -Mid should be comparable, while Bionate-High will produce more aggressive wear, if stiffness or modulus is the dictating factor. The effect of material stiffness will be discussed in Chapter 4.

This study did not include the compressive strength of the Bionate grades. It was difficult to generate a specimen of sufficient size that would permit proper assessment of strength. Moreover, as this study was aimed at examining cartilage wear, the only relevant property with respect to Bionate is Young's modulus. Regarding the relevance of strength of these biomaterials, this would eventually need to be addressed. However we did not note any failure, at least microscopically on the pins following testing.

3.5 Conclusion

The TGA and DSC results gave insight into the effect of temperature on all three grades of Bionate. Bionate-Low, -Mid and -High were all stable at body temperature (37°C) which makes the material desirable for orthopaedic implants. Each material was also stable at mould temperature of 200°C which made for better fabrication of implants. The compressive loading test showed Bionate-Low to have the lowest Young's moduli value which accords with material hardness. There was an increase in Young's moduli as the Shore hardness of Bionate increased.

3.6 References

1. Giboz J, Copponnex T, Mélé P. Microinjection molding of thermoplastic polymers: a review. *J Micromechanics Microengineering*. 2007;17(6):R96. DOI: 10.1088/0960-1317/17/6/R02.
2. Scholes SC, Burgess IC, Marsden HR, Unsworth A, Jones E, Smith N. Compliant Layer Acetabular Cups: Friction Testing of a Range of Materials and Designs for a New Generation of Prosthesis that Mimics the Natural Joint. *Proc Inst Mech Eng [H]*. 2006;220(5):583–96. DOI: 10.1243/09544119H06404.
3. Geary C, Birkinshaw C, Jones E. Characterisation of Bionate polycarbonate polyurethanes for orthopaedic applications. *J Mater Sci Mater Med*. 2008;19(11):3355–63. DOI: 10.1007/s10856-008-3472-8.
4. Geary C, Jones E, Fitzpatrick D, Kelly CP, Birkinshaw C. In-vitro evaluation of a polyurethane compliant-layer glenoid for use in shoulder arthroplasty. *Proc Inst Mech Eng [H]*. 2010;224(4):551–63. DOI: 10.1243/09544119JEIM626.
5. Flannery M, Flanagan S, Jones E, Birkinshaw C. Compliant layer knee bearings: Part I: Friction and lubrication. *Wear*. 2010;269(5–6):325–30. DOI: 10.1016/j.wear.2010.04.001.
6. Liu Z, Chen Y, Ding W, Zhang C. Filling behavior, morphology evolution and crystallization behavior of microinjection molded poly(lactic acid)/hydroxyapatite nanocomposites. *Compos Part Appl Sci Manuf*. 2015;72:85–95. DOI: 10.1016/j.compositesa.2015.02.002.
7. Khan I, Smith N, Jones E, Finch DS, Cameron RE. Analysis and evaluation of a biomedical polycarbonate urethane tested in an in vitro study and an ovine arthroplasty model. Part I: materials selection and evaluation. *Biomaterials*. 2005;26(6):621–31. DOI: 10.1016/j.biomaterials.2004.02.065.

8. Ghail NNA, Little EG. Determination of the mechanical properties of Bionate 80A and Bionate 75D for the stress analysis of cushion form bearings. *Proc Inst Mech Eng [H]*. 2008;222(5):683–94. DOI: 10.1243/09544119JEIM372.
9. DSM. Bionate Thermoplastic Polycarbonate Polyurethane (PCU). Available at [http://www.dsm.com/content/dam/dsm/medical/en_US/documents/bionate\(r\)-pcu-product-sheet.pdf](http://www.dsm.com/content/dam/dsm/medical/en_US/documents/bionate(r)-pcu-product-sheet.pdf).
10. Cipriani E, Zanetti M, Brunella V, Costa L, Bracco P. Thermoplastic polyurethanes with polycarbonate soft phase: effect of thermal treatment on phase morphology.
11. Cheremisinoff. *Handbook of Polymer Science and Technology*. CRC Press; 1989.
12. Streitberger H-J, Dossel K-F. *Automotive Paints and Coatings*. John Wiley & Sons; 2008.
13. Guo J, Zhao M, Ti Y, Wang B. Study on structure and performance of polycarbonate urethane synthesized via different copolymerization methods. *J Mater Sci*. 2007;42(14):5508–15. DOI: 10.1007/s10853-006-1024-5.
14. DSM Polyurethane Injection Molding Guide: Confidential 2014.
15. Simmons A, Hyvarinen J, Odell RA, Martin DJ, Gunatillake PA, Noble KR, et al. Long-term in vivo biostability of poly(dimethylsiloxane)/poly(hexamethylene oxide) mixed macrodiol-based polyurethane elastomers. *Biomaterials*. 2004;25(20):4887–900. DOI: 10.1016/j.biomaterials.2004.01.004.

Chapter 4

The Effect of Low Moduli Implant Biomaterials on Early *In Vitro* Cartilage Wear

Overview: *This chapter focuses on the in vitro performance of the three Bionate formulations (Bionate-Low, Bionate-Mid and Bionate-High) and ceramic on the wear of bovine cartilage specimens. A pin-on-plate wear simulator was employed. Using a previously validated imaged-based technique, wear volume and depth was quantified throughout testing up to 50,000 cycles.*

4.1 Introduction

As discussed in Chapter 1 (Section 1.2), hemiarthroplasty procedures are viable alternatives to total joint replacement in cases where only one articulating side of a synovial joint is damaged. Complication and failure rates are much higher in upper limbs than lower limbs for total arthroplasty because of the invasive surgical techniques that are performed for implantation of artificial joints^{1,2}. Hemiarthroplasty procedures help to reduce complication and failure by maximizing bone preservation, restoring joint function and stability through less invasive surgical techniques³. These procedures are able to simplify the surgical approach, reduce costs and preserve native anatomy but the cartilage wear associated with these types of implants create suboptimal clinical outcomes.

Most clinically used hemiarthroplasty implants are made from cobalt chromium or stainless steel. Literature has suggested that the high stiffness associated with these hemiarthroplasty implant materials are causing problems long term due to the decreased articular contact area and increased cartilage stress, which leads to damage of the adjacent articular cartilage⁴. *In vivo* studies have reported that the longevity of hemiarthroplasty implants is limited by wear because there is a correlation between length of time an implant is in place and the severity of articular cartilage wear⁵⁻⁷. The improvement of implant-cartilage contact mechanics is necessary to improve hemiarthroplasty implant longevity and performance⁸⁻¹⁰.

A study was conducted by Khayat¹⁰ to understand the effect of hemiarthroplasty implant material on early *in vitro* cartilage wear. The softest material that was studied against bovine cartilage was ultra high molecular weight polyethylene, which had a Young's modulus value of 0.69 GPa. There were no significant differences measured in volumetric cartilage wear when comparing stainless steel, titanium, high-density polyethylene, and ultra high molecular weight polyethylene. The author concluded that the stiffness did not have an effect on articular cartilage wear because of the relatively high moduli for the range of materials tested when compared to cartilage.

The purpose of this study was to investigate the effect of low hemiarthroplasty implant stiffness (down to 0.020 GPa) on cartilage wear. Hemiarthroplasty implant models were made from the three grades of Bionate with Young's moduli ranging from 0.020 to 0.222 GPa, as described in Chapter 3. The implants were reciprocated against bovine articular cartilage plugs in a pin-on-plate wear simulator to determine the relationship between material stiffness and *in vitro* cartilage wear. Implant performance was evaluated in terms of volumetric wear and wear depth. It was hypothesized that decreasing the implant stiffness will reduce cartilage wear because of improved contact mechanics.

4.2 Materials and Methods

4.2.1 Implant Models

Bionate pins (Bionate-Low, Bionate-Mid, and Bionate-High) with a radius of curvature of 4.7 mm were selected as the hemiarthroplasty implant models. The pins were attached on to a screw and coupling nut jig to fit into the pin-on-plate wear simulator (Figure 4-1). The three Bionate implant pins were made through the process of microinjection moulding as discussed in Chapter 3. The pins were washed using a diluted isopropyl alcohol solution to remove moulding lubricant and any debris from the pin surface.

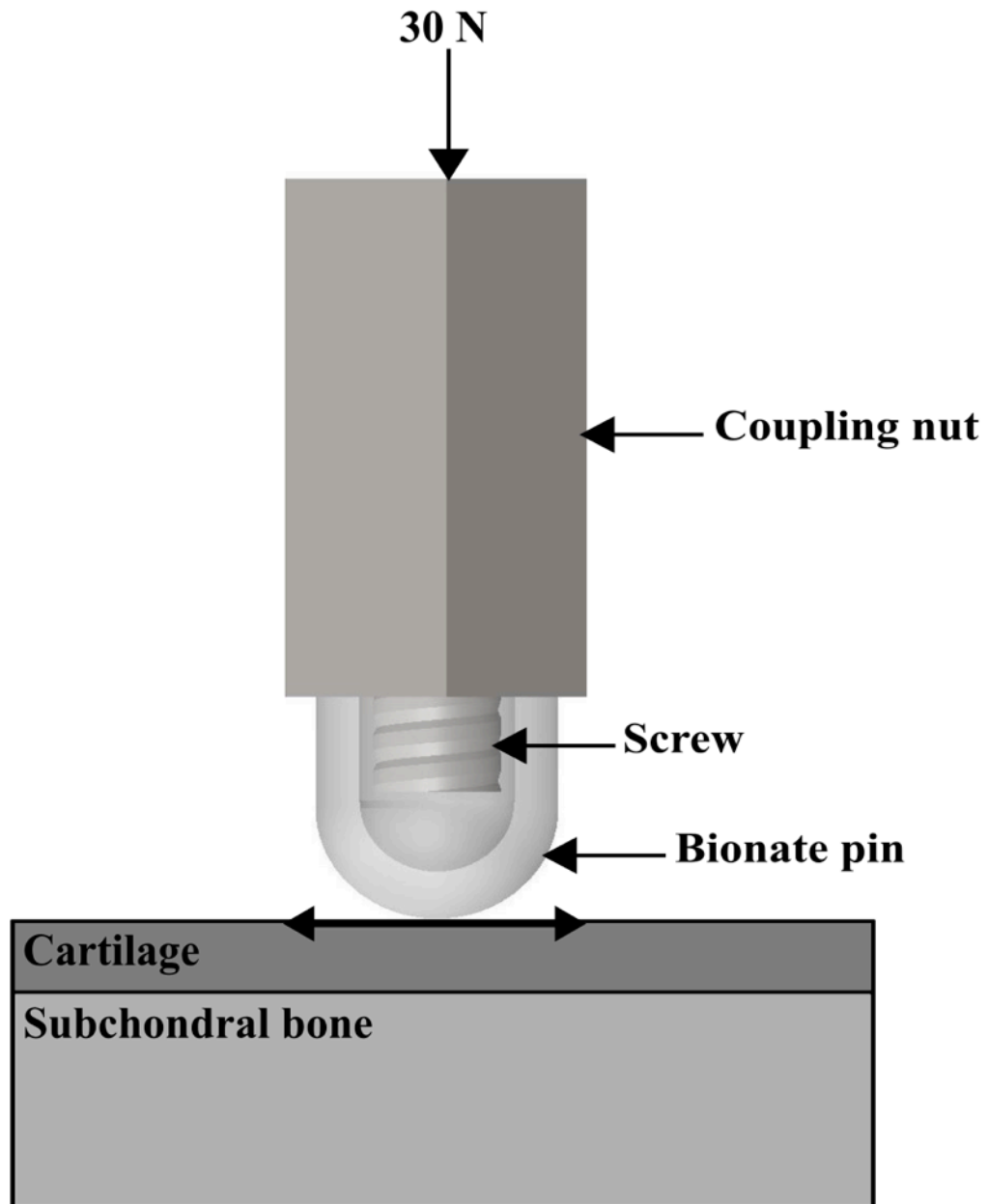


Figure 4-1 Configuration of the pin-on-plate wear simulator: The Bionate pin was threaded on to the screw and coupling nut jig. A constant load of 30 N was applied to the cartilage surface via the implant model.

The procedure for determining the Young's moduli of each Bionate implant was described in Chapter 3. The average surface roughness was measured using a Veeco Wkyko NT1100 optical profiler (Plainview, New York) to determine if differences in cartilage wear could be attributed to surface finish. The surface roughness average for each implant material is shown in Table 4-1. There was no significant difference in surface roughness average among the Bionate implants ($p>0.05$).

Table 4-1: Surface roughness average for the four implant materials tested

Implant Material	Surface Roughness Average, R_a [μm]
Bionate-Low	1.07±0.04
Bionate-Mid	1.15±0.21
Bionate-High	0.94±0.28
Ceramic (Si_3N_4)	0.02

4.2.2 Tissue Acquisition and Preparation

Bovine ulnae and radii obtained from a local abattoir (Ralph Bos Meats Ltd, Strathroy, ON) were frozen at -20°C within 12 hours of death. Similar specimens have been tested previously in our laboratory¹⁰. Studies have shown that freezing cartilage specimens at -20°C and thawing the specimens does not alter the mechanical properties of articular cartilage¹⁰⁻¹⁴.

Cylindrical plugs of cartilage and subchondral bone were harvested from the proximal faces of the ulnae and radii once the specimen was thawed. A diamond-tip hole saw with a diameter of 25 mm was used to extract 5 mm deep cylindrical plugs of cartilage and underlying subchondral bone, one each from the radial and ulnar sides of the bovine joint. The specimens were randomly placed in the wear simulator. The cartilage specimens were potted into custom jigs using Instant Tray Mix (Lang Dental Manufacturing Co.,

Inc., Illinois). The cartilage surfaces were scanned before wear testing using a non-contact 3D scanner (NextEngine, Santa Monica, California). The cartilage specimens were submerged in phosphate buffered saline and placed in a sealed bag and stored in a refrigerator at 4°C the night before testing.

4.2.3 Wear Testing

The cartilage plugs were submerged in a lubricant consisting of HyClone™ Alpha Calf Fraction Serum Supplement (GE Healthcare Life Sciences, Utah, USA) with an original protein concentration of 38 g/L¹⁵, which was diluted with phosphate buffered saline to a final protein concentration of 17 g/L in accordance with ISO standards¹⁶. The lubricant also contained 1% concentration of Antibiotic-Antimycotic (Invitrogen, Missisauga, ON). Alpha calf serum was used because it has similar protein constituent fractions to synovial fluid¹⁷. The wear test experiments were conducted at room temperature (22°C).

Testing on the cartilage specimens was conducted using the six-station pin-on-plate wear simulator in linear reciprocal sliding in the flexion-extension axis. A load of 30 N was applied to the pins. The number of specimens for each group were as follows: $n=6$ for Bionate-Low, $n=6$ for Bionate-Mid, $n=5$ for Bionate-High, and $n=5$ for ceramic. The pins reciprocated against the cartilage plugs at a frequency of 1.2 Hz and a total stroke length of 10 mm for a total of 50,000 cycles.

4.2.4 Wear Quantification

The volume of cartilage removed during wear testing was employed as the metric to quantify cartilage wear. Volumetric wear was measured by comparing three-dimensional scans taken of the cartilage plugs before and after wear testing at 10,000, 20,000, 30,000, and 50,000 cycles.

After testing, the worn specimens were stained with India ink because it can identify the extent and severity of fibrillation on the cartilage surface because the ink has a high affinity for fibrillation, which is a clear indicator of wear¹⁸. Excess ink was wiped off by using a damp cloth and the damaged areas were identified by where the ink adhered to the fibrillated cartilage.

The cartilage plugs were re-scanned using the 3D scanner under identical settings to the scans taken before testing. The macro range setting for the scanner was used, which produced a point cloud with 0.127 mm accuracy and containing 26 points/mm². Each point cloud was exported as a mesh with triangular elements and 0.191 mm element length. The full-colour scans were exported as meshes in .ply extension format.

Four landmarks on each cartilage plug surface were used as references to align the pre- and post- wear scans in MeshLab. A threshold filter was applied to the merged mesh in ParaView to determine the worn and unworn surfaces. The two surfaces were then opened in 3D Slicer where the Model-to-Model distance extension was used to determine the distance between the two surfaces. The new distance model was opened in ParaView where the wear track was selected and exported as a .vtk file. A custom written VTK algorithm, previously used by Khayat¹⁰, was used to calculate the distance between the vertices of the triangular element meshes in MATLAB (see Appendix A). The vertices with the same coordinates had a distance of zero between them and therefore represented the unworn regions. The distance between corresponding points on the registered surfaces indicated the depth of wear in the worn regions. The total volumetric wear was calculated by taking the area of each triangular mesh element and multiplying by the normal distance from the centroid of each triangular element, and then summed over the entire surface.

The data was analyzed using a two way ANOVA to determine if significant differences were observed based on material and number of wear cycles.

4.3 Results

Volumetric wear (mean \pm one standard deviation) are shown in Figure 4-2 for Bionate-Low, -Mid, -High, and ceramic implant models. Of the three materials investigated in this study, Bionate-High and ceramic produced visible evidence of cartilage wear across all specimens tested. There was no significant change in volumetric wear between Bionate-Low and Bionate-Mid ($p>0.05$). There was also no significant change in volumetric wear between Bionate-High and ceramic ($p>0.05$). Bionate-Low had significantly less volumetric wear ($p<0.001$) than Bionate-High and ceramic. Bionate-Mid also had significantly less volumetric wear ($p<0.001$) than Bionate-High and ceramic.

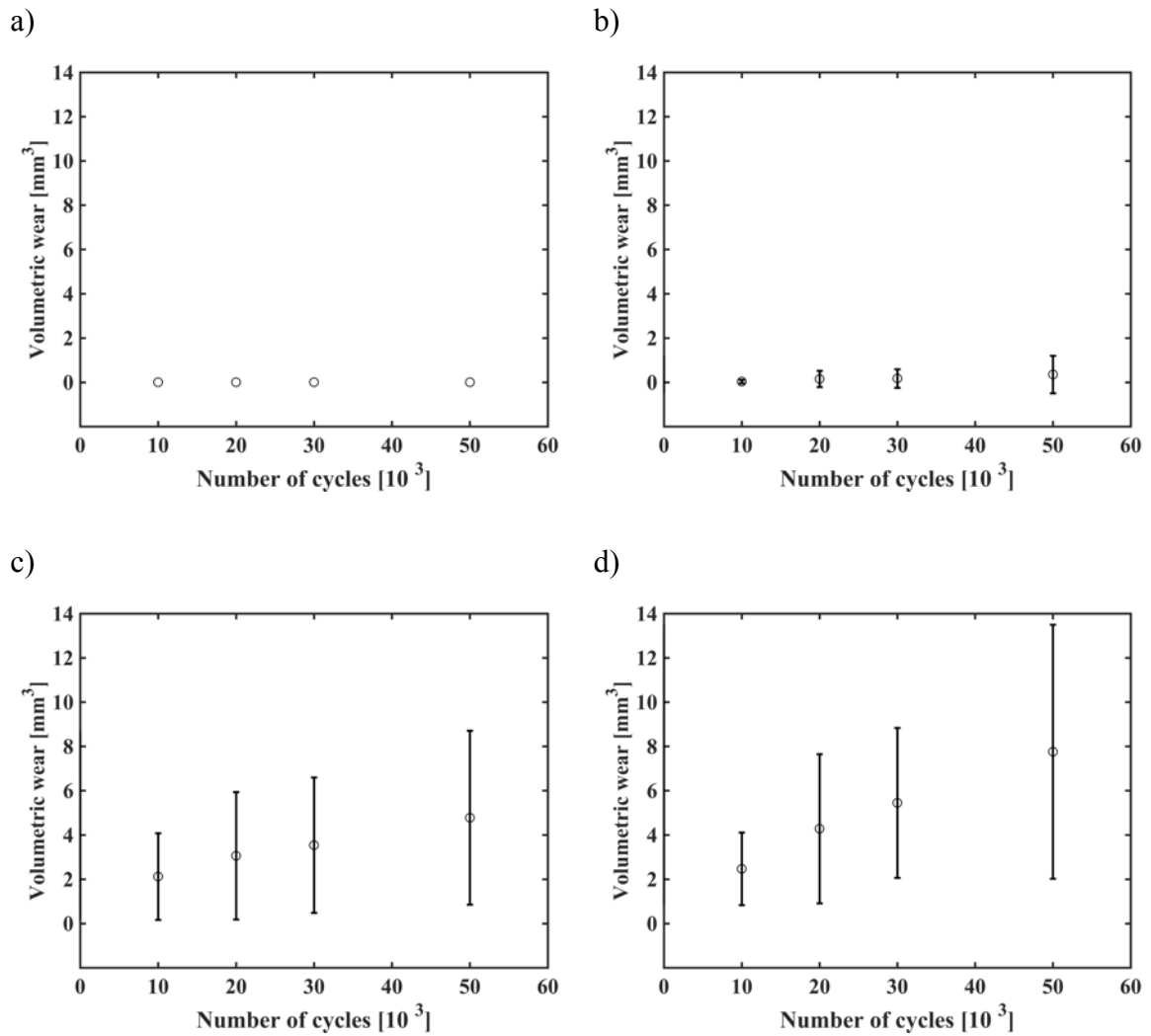


Figure 4-2: Mean (\pm one standard deviation) volumetric wear for: a) Bionate-Low b) Bionate-Mid c) Bionate-High and d) ceramic. Bionate-High and ceramic produced significantly more wear than Bionate-Low and Bionate-Mid ($p < 0.001$).

Figure 4-3 shows that after 50,000 cycles there is an increase in volumetric wear as the implant stiffness increases. There was a significant change in volumetric wear ($p < 0.05$) between 10,000 and 50,000 cycles.

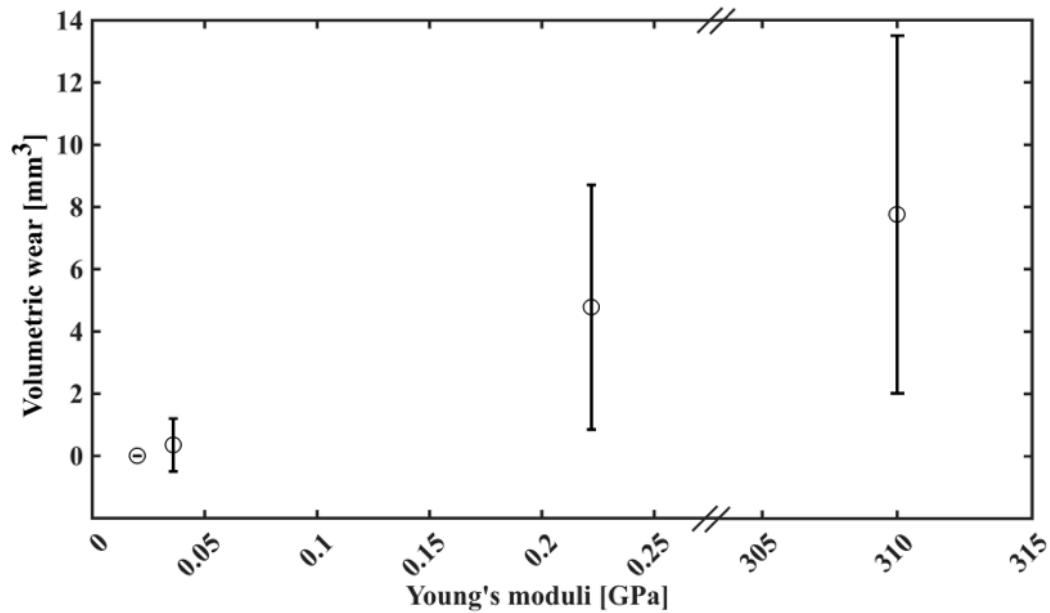


Figure 4-3: Mean (\pm one standard deviation) volumetric wear after 50,000 cycles for each implant material. Volumetric wear significantly increased between 10,000 and 50,000 cycles ($p < 0.05$).

The wear depths were calculated for each implant material across the four wear cycles. The average wear depth was determined by dividing the volumetric wear by the measured contact areas at the implant-cartilage interface using the casting technique (see Appendix B). Wear depth (mean \pm one standard deviation) are shown in Figure 4-4 for Bionate-Low, -Mid, -High, and ceramic. There was no significant change in wear depth between Bionate-Low and Bionate-Mid ($p>0.05$). There was also no significant change in wear depth between Bionate-High and ceramic ($p>0.05$). Bionate-Low produced significantly shallower cartilage wear tracks ($p<0.001$) than Bionate-High and ceramic. Bionate-Mid had a significantly shallower wear depth ($p<0.001$) than Bionate-High and ceramic.

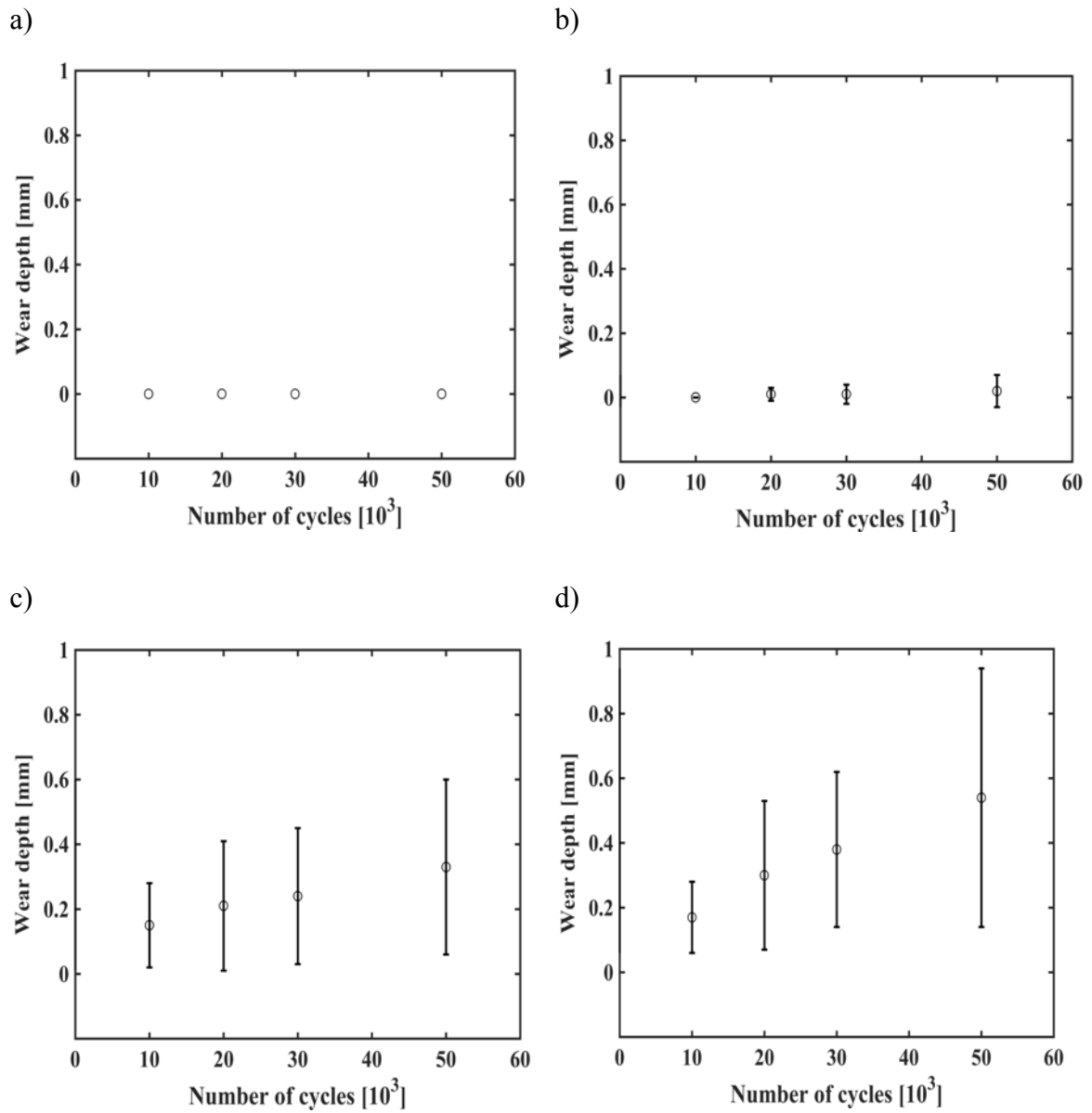


Figure 4-4: Mean (\pm one standard deviation) wear depth for: a) Bionate-Low b) Bionate-Mid c) Bionate-High and d) ceramic. Bionate-High and ceramic produced significantly deeper wear tracks in the cartilage plugs ($p < 0.001$).

4.4 Discussion

Volumetric wear has been quantified by mass difference in samples, India ink, and nuclear magnetic resonance (NMR). The difference in specimen mass before and after wear testing can be difficult to execute and inaccurate due to the high water content in cartilage. The “gold standard” to quantify cartilage wear is determining the amount of cartilage removed based on the protein content found in the lubricant and then expressing it as a function of the cartilage’s original surface volume or area. The mass of cartilage removed during wear testing can be inferred from the hydroxyproline content in the lubricating fluid based on the assumption that this protein accounts for 7.8% of bovine cartilage dry weight¹⁸.

India ink is used in semi-quantitative cartilage wear assessment. McGann et al. reported a high correlation between wear rates measured using India ink staining protocol and the “gold standard” protocol¹⁸. The wear tracks were stained by India ink to visualize the damaged cartilage. Images were taken with a dissection microscope and the black and white pixel images were imported into MATLAB and a threshold technique was applied. The number of black pixels were counted and converted into an area, which represented the area of cartilage damage. The stained areas were normalized to account for differences between the contact areas to yield a percentage of the specimen contact area that had been damaged¹⁸. The use of India ink was deemed an effective, inexpensive and quick technique for evaluating cartilage degradation and thus making it a sufficient alternative to mass difference analysis.

Volumetric wear has also been measured using NMR. Vertical magnet scans of the worn cartilage surface have been taken and a curve fitting program is used to estimate the unworn cartilage surface topography based on the perimeter geometry of the wear track¹⁹. NMR is not always the most optimal solution because it takes a long time to process and there is possible error in the curve-fitting program. We opted to use a non-contact 3D scanner in our wear study because it would enable a direct comparison between 3D meshes generated from before and after scans of the cartilage surface without risking cartilage degradation.

The purpose of this study was to determine cartilage wear for the different implant materials studied. The load employed for this experimental analysis was the same as the computational analysis (FEA) discussed in Chapter 2. As previously discussed, hemiarthroplasty procedures reduce articular contact area, which leads to an increase in contact stress. It was important to choose a load that would produce contact stress levels within the clinically relevant range for various hemiarthroplasty procedures. Post-operative contact stresses have been reported as 2.28 MPa²⁰ in shoulder hemiarthroplasty (humeral head implant against glenoid) procedures, 5.4 MPa²¹ in elbow hemiarthroplasty (radial head implant against capitellum) procedures and 10 MPa²² in hip hemiarthroplasty (femoral head implant against acetabulum) procedures. The finite element model showed that Bionate-Low, -Mid, -High and ceramic should produce stresses within this clinical range of 2.28-10 MPa.

Overall, the data showed that there is a clear relationship between implant stiffness and early *in vitro* cartilage wear. It is interesting to note that there was very little to no wear with Bionate-Low and Bionate-Mid, strongly suggesting that there may be a threshold of contact area/stress that initiates wear of cartilage. It would thus seem that implants with a modulus of approximately 0.035 GPa or less might produce no wear, at least in the early stages.

The Bionate-High and ceramic implants produced the smallest contact area at the implant-cartilage interface and produced the largest amount of volumetric wear. The amount of volumetric wear could have been caused by the increase in contact stress magnitudes that result from a decrease in contact area. The large standard deviations measured in the Bionate-High and ceramic wear results could have been a result of cartilage variation. Both Bionate-High and ceramic implants showed an increase of average volumetric wear over 50,000 cycles. With there being no significant change in volumetric wear ($p > 0.05$) and wear depth ($p > 0.05$) between these two materials, despite the very large difference in the modulus of elasticity, suggests that there is not a linear relationship between wear and stiffness, and there is a threshold level as noted above. Further biomaterials will need to be studied to determine the optimal Young's moduli range for hemiarthroplasty implants.

Out of the six Bionate-Mid specimens studied, volumetric wear was only detected on one cartilage specimen. This wear could have been caused by material attaching to the implant surface therefore making the implant material more abrasive.

There are some limitations with using a pin-on-plate wear simulator to conduct *in vitro* wear testing. The apparatus is unable to replicate native joint motion and *in vivo* joint geometry. The duration of testing was relatively short (purpose was to gain information on early *in vitro* cartilage wear) and the cartilage specimens were harvested from bovine versus human specimens. A constant load was applied across each specimen and therefore future studies could be conducted to investigate the affect of varying load on volumetric cartilage wear. *In vivo* physiological processes such as cellular activity and inflammatory responses were not simulated by this study.

4.5 Conclusion

The data suggests that using Bionate-Low and Bionate-Mid as a potential hemiarthroplasty implant material improves contact mechanics that result from increasing the cartilage-implant contact area while reducing peak contact stress at the implant-cartilage interface. Bionate-High produced increasing amounts of volumetric wear, which indicates that Bionate-High is too stiff of a material to improve contact mechanics. Perhaps the most impactful finding of this study is that modulus threshold likely exists with regard to wear, and this would appear to be approximately 0.020-0.035 GPa for at least the loading level modeled herein. This study does strongly suggest that implant materials such as polyethylene (Young's moduli of ~ 0.7 -2 GPa), polyetheretherketone (Young's moduli of ~ 4 GPa) and other materials in the same modulus range do not, in all likelihood, reduce wear relative to cobalt chromium implants, despite that thought trend in the orthopaedic industry. It would hence seem that hemiarthroplasty devices should be only considered if they have a modulus 0.035 GPa or less if reduced cartilage wear is desired.

4.6 References

1. Wright TW, Wong AM, Jaffe R. Functional outcome comparison of semiconstrained and unconstrained total elbow arthroplasties. *J Shoulder Elbow Surg.* 2000;9(6):524–31. DOI: 10.1067/mse.2000.109408.
2. Gschwend N. Present State-Of-The-Art in Elbow Arthroplasty. *Acta Orthop Belg.* 2002;68(2):100–17.
3. Klaus J Burkhart SN. Distal Humerus Hemiarthroplasty of the Elbow for Comminuted Distal Humeral Fractures in the Elderly Patient. *J Trauma.* 2011;71(3):635–42. DOI: 10.1097/TA.0b013e318216936e.
4. Liew VS, Cooper IC, Ferreira LM, Johnson JA, King GJW. The effect of metallic radial head arthroplasty on radiocapitellar joint contact area. *Clin Biomech.* 2003;18(2):115–8. DOI: 10.1016/S0268-0033(02)00172-9.
5. Dalldorf PG, Banas MP, Hicks DG, Pellegrini VD. Rate of degeneration of human acetabular cartilage after hemiarthroplasty. *J Bone Jt Surg.* 1995;77(6):877–82.
6. Cruess RL, Kwok DC, Duc PN, Lecavalier MA, Dang GT. The response of articular cartilage to weight-bearing against metal. A study of hemiarthroplasty of the hip in the dog. *J Bone Joint Surg Br.* 1984;66–B(4):592–7.
7. van Riet RP, Glabbeek FV, Verborgt O, Gielen J. Capitellar Erosion Caused by a Metal Radial Head Prosthesis. *J Bone Jt Surg Am.* 2004;86(5):1061–4.
8. Irish SE, Langohr GDG, Willing R, King GJ, Johnson JA. Implications of radial head hemiarthroplasty dish depth on radiocapitellar contact mechanics. *J Hand Surg.* 2015;40(4):723–9. DOI: 10.1016/j.jhsa.2015.01.030.
9. Langohr GDG, Willing R, Medley JB, King GJW, Johnson JA. The Effect of Radial Head Hemiarthroplasty Geometry on Proximal Radioulnar Joint Contact Mechanics. *J Hand Surg.* 2016;41(7):745–52. DOI: 10.1016/j.jhsa.2016.05.001.

10. Khayat A. Effect of Hemiarthroplasty Implant Contact Geometry and Material on Early Cartilage Wear. *Electron Thesis Diss Repos*. 2015.
11. Radin EL, Paul IL. Response of Joints to Impact Loading. I. In Vitro Wear. *Arthritis Rheum*. 1971;14(3):356–62. DOI: 10.1002/art.1780140306.
12. Szarko M, Muldrew K, Bertram JE. Freeze-thaw treatment effects on the dynamic mechanical properties of articular cartilage. *BMC Musculoskelet Disord*. 2010;11:231. DOI: 10.1186/1471-2474-11-231.
13. Radin EL, Swann DA, Paul IL, Mcgrath PJ. Factors influencing articular cartilage wear in vitro. *Arthritis Rheum*. 1982;25(8):974–80. DOI: 10.1002/art.1780250810.
14. Changoor A, Fereydoonzad L, Yaroshinsky A, Buschmann MD. Effects of Refrigeration and Freezing on the Electromechanical and Biomechanical Properties of Articular Cartilage. *J Biomech Eng*. 2010;132(6):064502–064502. DOI: 10.1115/1.4000991.
15. GE HealthCare HC. Certificate of analysis. 2012.
16. ISO-14243-3. Implants for surgery: Wear of total knee joint prosthesis. Part 3: Loading and displacement parameters for wear testing machines with displacement control and corresponding environmental conditions for test. 2004.
17. Brandt J. *Wear and boundary lubrication in modular total knee replacements*. 2008.
18. McGann ME, Vahdati A, Wagner DR. Methods to assess in vitro wear of articular cartilage. *Proc Inst Mech Eng [H]*. 2012;226(8):612–22. DOI: 10.1177/0954411912447014.
19. Luo Y, McCann L, Ingham E, Jin Z-M, Ge S, Fisher J. Polyurethane as a potential knee hemiarthroplasty biomaterial: An in-vitro simulation of its tribological performance. *Proc Inst Mech Eng [H]*. 2010;224(3):415–25. DOI: 10.1243/09544119JEIM657.

20. Petraglia CA, Ramirez MA, Tsai MA, Parks BG, Murthi AM. Glenohumeral Pressure With Surface Replacement Arthroplasty Versus Hemiarthroplasty. *Orthopedics*. 2014;37(10):e892–6. DOI: 10.3928/01477447-20140924-55.
21. Sahu D, Holmes DM, Fitzsimmons JS, Thoreson AR, Berglund LJ, An K-N, et al. Influence of radial head prosthetic design on radiocapitellar joint contact mechanics. *J Shoulder Elb Surg Am Shoulder Elb Surg Al*. 2014;23(4):456–62. DOI: 10.1016/j.jse.2013.11.028.
22. Anderson AE, Ellis BJ, Maas SA, Peters CL, Weiss JA. Validation of finite element predictions of cartilage contact pressure in the human hip joint. *J Biomech Eng*. 2008;130(5):51008. DOI: 10.1115/1.2953472.

Chapter 5

Conclusions and Recommendations

5.1 Findings Related to Objectives & Hypotheses

This work investigated the effect of low stiffness biomaterials on hemiarthroplasty contact mechanics using a finite element model and *in vitro* wear tests. The data presented in this body of work met the objectives that were stated in Chapter 1 (Section 1.7.1). To reiterate, the objectives were:

1. To develop and employ a finite element model to assess the effect of low modulus implants in the range of 0.015-0.288 GPa on cartilage contact area and peak contact stress (Chapter 2).
2. To develop an efficient and effective way to fabricate Bionate hemispherical-tipped implants and to characterize the chemical and mechanical properties of Bionate implants (Chapter 3).
3. To quantify the effect of varying Bionate implant stiffness on early *in vitro* cartilage wear (Chapter 4).

The findings from the studies conducted in Chapters 2, 3 and 4 are reviewed below.

In Chapter 2, a three-dimensional finite element model was constructed to determine peak contact stress and contact area of the low modulus Bionate implants investigated in this work. There was a decrease in peak contact stress and increase in contact area at the implant-interface with a decrease in implant modulus. Moreover, this data revealed the rapid change in contact mechanics (*viz.* area and stress) that occurs as the modulus is lowered in the range that approaches cartilage modulus.

In Chapter 3, microinjection moulding successfully fabricated Bionate[®] hemispherical-tipped implants. Chemical and mechanical testing was conducted on the implants to characterize the implant properties. The TGA results concluded that Bionate-Low, -Mid and -High were stable at body temperature, which makes the material reasonable for

hemiarthroplasty applications. The results from compressive loading suggested that Bionate-Low and Bionate-Mid might have comparable wear characteristics because of their similar Young's moduli values.

Chapter 4 focused on the *in vitro* wear studies. Even though Bionate-High has a much lower Young's modulus (0.2 GPa) than currently used hemiarthroplasty implant materials, it was demonstrated that a stiffness of roughly 0.2 GPa still causes significant cartilage wear. Based on the wear testing results, implants with a Young's moduli of approximately 0.035 GPa or less will be required to reduce cartilage wear. The decrease in peak stress with lower implant stiffness shown by the finite element simulation corroborates the reduction in average volumetric wear presented in Chapter 4. The Bionate-Low model showed the lowest peak contact stress and resulted in no visible cartilage wear during *in vitro* wear testing. Within the range of low stiffness materials examined, lower peak contact stress and higher contact area were observed as the Young's moduli decreased which indicates that a material with similar characteristics to cartilage optimizes contact mechanics and decreases cartilage wear.

Two hypotheses were formulated at the beginning of this investigation (Section 1.7.2). The first hypothesis stated the finite element model would show an increase in contact area and a decrease in peak contact stress at the implant-cartilage interface with a decrease in implant Young's moduli. This hypothesis was hence accepted based on moduli below 0.038 GPa resulting in an increase in contact area and a decrease in peak contact stress. The second hypothesis stated that decreasing implant stiffness would reduce wear on the articulating cartilage because of improved contact mechanics. This hypothesis was accepted based on the significant decrease in cartilage wear observed for Bionate-Low and Bionate-Mid ($p < 0.001$).

5.2 Recommendations for Future Work

The three-dimensional finite element model used published experimental Young's moduli and Poisson's ratio data. A more thorough validation of the model should be conducted using the experimental values determined from the compressive testing performed in Chapter 3. Contact areas determined in the finite element model could then

be compared to experimental contact areas measured from casts taken of the Bionate implant-cartilage interface and contact areas measured from Fuji Pressure Sensitive Film[®].

Using a three dimensional scanner to compare cartilage topography before and after wear testing allowed for quick and accurate capture of three dimensional cartilage meshes. India ink helped to quantify cartilage wear and make it visible on these cartilage meshes. To further develop this methodology for forthcoming investigations, these results can be compared to mass changes in cartilage plugs or compared to measured protein content of the lubricating bath after wear testing.

Further chemical and mechanical analysis can be done to increase material characterization. Additional chemical characterizations include water absorption and molecular weight of Bionate. Water absorption will help to better understand the lubrication abilities of Bionate in wear testing. Measuring the weight average molecular weight and the number average molecular weight to determine the polydispersity of Bionate will help indicate which mechanisms cause thermal degradation. Additional mechanical characterizations include compressive strength and fatigue strength should be tested. Compressive strength will provide insight into the maximum load that Bionate can withstand before failure. Determining the fatigue strength of Bionate will provide insight into the maximum stress Bionate can withstand during cyclic loading.

5.3 Conclusions

Even though hemiarthroplasty procedures have been clinically successful, they can cause progressive cartilage damage over time due to the use of relatively stiff metallic implant materials. This work investigated the role of a low stiffness implant material on implant-cartilage contact mechanics and early *in vitro* cartilage wear. Within the range of implant materials examined, a higher contact area and lower peak contact stress was observed using a finite element model as Young's moduli decreased, particularly when the modulus was below 0.04 GPa. An *in vitro* wear study demonstrated a significant decrease in cartilage wear for the 0.020 GPa and 0.035 GPa grades of Bionate ($p < 0.001$). In a qualitative sense, the *in vitro* wear studies mirrored the results of the computational finite

element modeling which suggest this material will be a major advance if incorporated into hemiarthroplasty implant designs.

In conclusion, these studies have demonstrated the desirable range of implant moduli to reduce cartilage wear, and have shown that Bionate has the potential to minimize cartilage wear for hemiarthroplasty constructs. These findings provide important and novel baseline information to set the stage for future explorations of low modulus materials to minimize or perhaps eliminate cartilage wear with hemiarthroplasty procedures. This is very timely and relevant, as less invasive implant systems are the goal for surgeons, biomechanists, and ultimately, patients.

Appendices

A. MeshLab Mesh Registration and MATLAB Volumetric Wear Calculation Protocols

This appendix describes the computational methods used to determine the volumetric wear between unworn and worn cartilage surface meshes.

The pre- and post-wear cartilage scans of each specimen were imported to MeshLab as .ply files. The “Align” tool was applied to fix the position of the pre-wear scan by selecting “Glue Here Mesh.” The post-wear scan was selected and the “Point Based Gluing” option was used. This tool allows the user to select four landmarks on the two surfaces to merge the meshes. “Processing” the mesh alignment completed the merging. This process was repeated until the mesh alignment error was below five percent. The “Flattening the visible layers” tool was then used and a single .ply format exported the mesh.

The merged mesh was then opened in ParaView (Kitware Inc, New York, USA) where the “Connectivity” filter was selected to separate the unworn and worn surfaces. A threshold function was applied to both surfaces and each surface was saved as a binary .vtk file. Both models were opened in 3D Slicer. The “Model-to-Model distance” extension was used to create a model that calculated the distance between the two surfaces. The file was exported in binary .vtk format and the colour-contour map was then opened in ParaView. Points were selected and extracted using the “Extract Selection” filter. The “Point Data to Cell Data” filter was applied to the model and exported in ASCII .vtk file format.

The MATLAB function (.m file format) that was written to compute volume between the two surfaces to determine the volumetric wear is shown in Figure A-1.

```

function [postive_volumes negative_volumes] = parse_surface_results(input_file)
% This program parses an input VTK surface and extracts the points and
% polys

% initialize incase they don't get filled;
Dist_data=[];

%Read in source surface info
fid=fopen(input_file,'r');

compare1=false;
compare2=false;

DIST=false;

while 1
    tline=fgetl(fid);
    compare1 = strncmpi(tline,'POINTS',6);
    compare2 = strncmpi(tline,'POLYGONS',8);
    compare3 = strncmpi(tline,'CELLS',5);
    DIST = strncmpi(tline,'SCALARS Distance',16);
    DIST2 = strncmpi(tline,'SCALARS Signed',14);

    if tline==-1
        break
    end

    if (compare1==true)
        npoints=sscanf(tline,'%s %i %s',[1]);
        fseek(fid,0,'cof');
        points=fscanf(fid,'%g',[3,npoints]);
    end

    if (compare2==true)
        npolys=sscanf(tline,'%s %i %s',[1]);
        fseek(fid,0,'cof');
        polys=fscanf(fid,'%i %i %i %i',[3,npolys]);
    end

    if (compare3==true)
        npolys=sscanf(tline,'%s %i %s',[1]);
        fseek(fid,0,'cof');
        polys=fscanf(fid,'%i %i %i %i',[3,npolys]);
    end

    if (DIST==true)||(DIST2==true)
        fseek(fid,0,'cof');
        temp=fgetl(fid);
        Dist_data=fscanf(fid,'%f');
    end
end

```

```

end

fclose(fid);

points=points';
polys=polys';

X=(points(polys(:,1)+1,1)+points(polys(:,2)+1,1)+points(polys(:,3)+1,1))/3;
Y=(points(polys(:,1)+1,2)+points(polys(:,2)+1,2)+points(polys(:,3)+1,2))/3;
Z=(points(polys(:,1)+1,3)+points(polys(:,2)+1,3)+points(polys(:,3)+1,3))/3;

centroids=[X Y Z];

V_1_X=points(polys(:,2)+1,1)-points(polys(:,1)+1,1);
V_1_Y=points(polys(:,2)+1,2)-points(polys(:,1)+1,2);
V_1_Z=points(polys(:,2)+1,3)-points(polys(:,1)+1,3);

V_1=[V_1_X V_1_Y V_1_Z];

V_2_X=points(polys(:,3)+1,1)-points(polys(:,1)+1,1);
V_2_Y=points(polys(:,3)+1,2)-points(polys(:,1)+1,2);
V_2_Z=points(polys(:,3)+1,3)-points(polys(:,1)+1,3);

V_2=[V_2_X V_2_Y V_2_Z];

NORM=cross(V_1,V_2,2);

areas=((NORM(:,1).*NORM(:,1)+NORM(:,2).*NORM(:,2)+NORM(:,3).*NORM(:,3)).^0.5)/2;

normals=NORM./[((NORM(:,1).*NORM(:,1)+NORM(:,2).*NORM(:,2)+NORM(:,3).*NORM(:,3)).^0.5)
((NORM(:,1).*NORM(:,1)+NORM(:,2).*NORM(:,2)+NORM(:,3).*NORM(:,3)).^0.5)
((NORM(:,1).*NORM(:,1)+NORM(:,2).*NORM(:,2)+NORM(:,3).*NORM(:,3)).^0.5)];

volumes=Dist_data.*areas;
postive_volumes=sum(volumes(find(volumes>0)));
negative_volumes=sum(volumes(find(volumes<0)));

```

Figure A-1: MATLAB function to determine volumetric wear between unworn and worn surface meshes

B. Experimental Implant-Cartilage Contact Area Determined from an Experimental Casting Technique

The contact area used to determine wear depth in Chapter 4 was measured using a casting technique. Silicone-based dental cement, Reprosil[®] (Dentsply International Inc., Milford, DE, USA) was allowed to cure between the implant and the cartilage under compressive loading to measure the contact area at the implant-cartilage interface. Three casts were created for each of the four-implant materials. The casts were scanned to create images that could be opened in Image J where the contact area was measured. The contact area results from the casting technique are displayed graphically in Figure B-1. The wear depth was calculated by dividing the volumetric wear by the contact area determined from the casts.

There was a 48-49% difference in contact area when comparing Bionate-Low to Bionate-High and ceramic. There was a 1.15% difference in contact area between Bionate-High and ceramic. The larger contact area exhibited by Bionate-Low further helps to explain the negligible volumetric wear during the wear testing, likely due to more favourable contact mechanics between the implant and the cartilage. This would also decrease peak contact stress at the implant-cartilage interface.

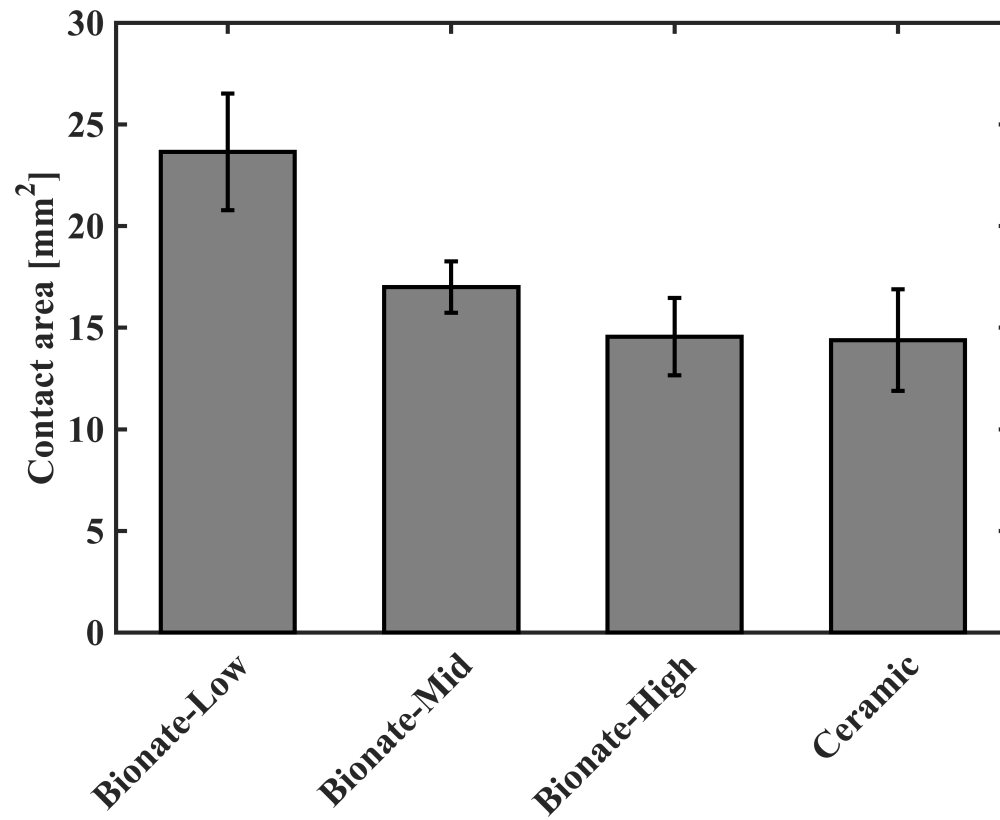


Figure B-1: Mean (\pm one standard deviation) contact area measurements from casting for the four implant materials

Curriculum Vitae

Name: Sarah DeDecker

Post-secondary Education and Degrees: The University of Western Ontario
London, Ontario, Canada
2010-2014 BEng, Chemical Engineering

Honours and Awards: Second Place Award in the Fuel & Energy Category at the 9th Annual Capstone Design Competition
Western Sarnia-Lambton Research Park
March 2014

Related Work Experience: Teaching Assistant
The University of Western Ontario
2014-2016

Western Engineering Research Student
The University of Western Ontario
2014

Research Assistant
Roth-McFarlane Hand and Upper Limb Centre
St. Joseph's Hospital
2013-2014, 2015-2016

Conference Presentations:

“Implications of Low Stiffness Biomaterials on Contact Mechanics of Joint Hemiarthroplasty”
Poster presented at the 2016 Annual Meeting of the Orthopaedic Research Society

“Low Moduli (<0.025 GPa) Hemiarthroplasty Implants May Restore Joint Contact Mechanics to the Native State”
Poster presented at the 2016 Canadian Bone and Joint Conference

“Implications of Low Stiffness Biomaterials on Contact Mechanics of Joint Hemiarthroplasty: A Finite Element Study”
Poster presented at the 2016 Annual Meeting of the Canadian Orthopaedic Association/Canadian Orthopaedic Research Society